Article

A 3D study of the photosphere of HD 99563 - I. Pulsation analysis

Freyhammer, L. M., Kurtz, D. W., Elkin, V. G., Mathys, G., Savanov, I., Zima, W., Shibahashi, H. and Sekiguchi, K.

Freyhammer, L. M., Kurtz, D. W. ORCID: 0000-0002-1015-3268, Elkin, V. G., Mathys, G., Savanov, I., Zima, W., Shibahashi, H. and Sekiguchi, K. (2009) A 3D study of the photosphere of HD 99563 - I. Pulsation analysis. Monthly Notices of the Royal Astronomical Society, 396 (1). pp. 325-342. ISSN 00358711

Mon. Not. R. Astron. Soc. **396,** 325–342 (2009) doi:10.1111/j.1365-2966.2009.14538.x

A 3D study of the photosphere of HD 99563 – I. Pulsation analysis⋆

L. M. Freyhammer,[1]† D. W. Kurtz,[1] V. G. Elkin,[1] G. Mathys,[2] I. Savanov,[1] W. Zima,[3] H. Shibahashi[4] and K. Sekiguchi[5]

[1]*Centre for Astrophysics, University of Central Lancashire, Preston PR1 2HE*
[2]*European Southern Observatory, Casilla 19001, Santiago 19, Chile*
[3]*Instituut voor Sterrenkunde, K.U. Leuven, Celestijnenlaan 200D, 3001 Leuven, Belgium*
[4]*Department of Astronomy, University of Tokyo, Tokyo 113-0033, Japan*
[5]*National Astronomical Observatory of Japan, Mitaka, Tokyo 181-8588, Japan*

Accepted 2009 January 21. Received 2009 January 21; in original form 2008 October 7

ABSTRACT

We have used high-speed spectroscopy of the rapidly oscillating Ap (roAp) star HD 99563 to study the pulsation amplitude and phase behaviour of elements in its stratified atmosphere over one 2.91-d rotation cycle. We identify spectral features related to patches in the surface distribution of chemical elements and study the pulsation amplitudes and phases as the patches move across the stellar disc. The variations are consistent with a distorted non-radial dipole pulsation mode. We measure a 1.6 km s^{-1} rotational variation in the mean radial velocities of Hα and argue that this is the first observation of Hα abundance spots caused by He settling through suppression of convection by the magnetic field on an oblique rotator, in support of a prime theory for the excitation mechanism of roAp star pulsation. We demonstrate that HD 99563 is the second roAp star to show aspect dependence of blue-to-red running wave line profile variations in Nd III spots.

Key words: stars: atmospheres – stars: chemically peculiar – stars: individual: HD 99563 – stars: magnetic fields.

1 INTRODUCTION

1.1 The Ap stars

Ap stars are chemically peculiar stars that range from early-B to early-F spectral types with the majority having detectable magnetic fields with strengths of a few 10^2 to a few 10^4 G (Bychkov, Bychkova & Madej 2003, according to whom ∼55 per cent have mean longitudinal fields greater than 400 G). The study of Ap stars with strong magnetic fields has ramifications for several other branches of astrophysics. The interaction among strong magnetic fields, atomic diffusion and energy transfer in (or above) the upper atmospheres of non-degenerate stars has direct implications for observed stellar abundances and for the instability of stellar pulsations in β Cephei and sdB stars. The very different magnetic field strengths, orientations and geometries, as well as the great variety of surface abundance distributions for Ap stars therefore make them particularly informative. The magnetic field geometry, determined from maps of longitudinal magnetic field strength versus rotation phase, generally agrees with an axisymmetric dipole, although strong deviations from this do occur, e.g. the quadrupole field configuration of HD 37776 (Thompson & Landstreet 1985). Typically, the magnetic axis is significantly inclined to the rotation axis, hence these stars are called oblique rotators.

Many Ap stars are known to have surface spots, indirectly observable from photometric light variations or spectroscopic line strength variations over a rotation cycle. These stars are known as α^2 CVn stars after the prototype of that name (Pyper 1969). Their light and line strength variations are a consequence of abundance spots that are often associated with the magnetic poles. The rotation period of Ap stars is typically relatively long – of the order of several days to years, and even in some cases decades, as determined from their magnetic field variations. Slow rotation is a requirement for the atmospheric atomic diffusion that gives rise to the observed spectral peculiarities, since rapid rotation generates turbulent meridional circulation that inhibits diffusion. Interestingly, atomic diffusion processes can give rise to observably stratified atmospheres in some Ap stars, and probably all rapidly oscillating Ap (roAp) stars. Examples of studies of atmospheric abundance stratification in the cool roAp star subgroup are given by Wade et al. (2001), Ryabchikova et al. (2002) and Ryabchikova, Leone & Kochukhov (2005).

These studies are in agreement with each other. In general, Fe is concentrated by gravitational settling in the deeper observable

⋆Based on observations collected at the European Southern Observatory (ESO), Paranal, Chile (programmes 072.D-0138, 078.D-0192), and at the Subaru Telescope, which is operated by the National Astronomical Observatory of Japan (programme S07A-005).

†E-mail: lmfreyhammer@uclan.ac.uk

layers in the photosphere around $\log \tau_{5000} \sim -0.5$; the Pr and Nd line-forming layers are concentrated by radiative levitation high in the atmosphere at $\log \tau_{5000} \leq -4$, a level that is chromospheric in the Sun, and in the roAp stars is above the line-forming layer of the narrow core of the Hα line at $-4 \leq \log \tau_{5000} \leq -2$, which is itself above the Fe line-forming layer. Many other elements show similar behaviour to these examples.

Doppler imaging studies of Ap stars show that the spots associated with the magnetic poles are typically caused by abundance concentrations of rare earth elements. Overabundances globally are several orders of magnitude compared to normal abundance stars (e.g. Adelman 1973), and may reach a factor of 10^8 in the spots, as shown by the Doppler imaging study of the roAp star HR 3831 by Kochukhov (2004), and as shown in this paper for HD 99563. As a result of these strong abundance anomalies, line-blocking changes the temperature gradient at the magnetic poles of Ap stars; flux is redistributed usually from the blue to the red, so that rotational light variations in visible light occur in antiphase for short and long wavelength observations, along with obvious spectral line strength variations. Importantly, the rotational variations – whether magnetic, spectroscopic or photometric – allow the precise determination of the stellar rotation period.

With the surface of some Ap stars resolvable by Doppler imaging, and atmospheric depth being resolved because of stratification, Ap stars – and particularly the roAp stars – offer the only opportunity for 3D studies of stellar atmospheres for any stars other than the Sun.

1.2 The roAp stars

A subgroup of Ap stars, the roAp stars, exhibits rapid oscillations with periods of 5–21 min. Their frequencies are considerably higher than those typical for δ Sct stars with whom they overlap in location inside the classical instability strip of the Hertzsprung-Russell (HR) diagram. At present, only 40 roAp stars are known (see e.g. Kurtz et al. 2006b; González et al. 2008), although several photometric surveys have searched for rapid pulsation in Ap stars, such as Nelson & Kreidl (1993); Martinez & Kurtz (1994); Handler & Paunzen (1999); Ashoka et al. (2000); Weiss et al. (2000); Dorokhova & Dorokhov (2005). For a (non-exhaustive) list of spectroscopic studies of roAp stars, see Kurtz, Elkin & Mathys (2006a).

The roAp class characteristics are therefore poorly constrained. As they share the same region of the HR diagram with the (photometrically established) non-oscillating Ap (noAp) stars, the selection of new roAp candidates is difficult and mostly leads to null results for both spectroscopic studies (see e.g. Elkin et al. 2008a; Freyhammer et al. 2008a; Freyhammer, Elkin & Kurtz 2008b) and for the photometric surveys listed above. The pulsations of roAp stars are described well by the oblique pulsator model, where the pulsation axis is assumed to be aligned with an oblique magnetic field axis (Kurtz 1982; Saio 2005), or derived to be offset from both the rotational and magnetic axes (Bigot & Dziembowski 2002).

Balmforth et al. (2001) used this model and assumed that convection was suppressed locally in the magnetic polar regions. They showed that pulsation aligned with the magnetic poles is unstable to the axisymmetric, non-radial high-order modes observed in roAp stars, mainly through excitation by the opacity (κ) mechanism acting in the hydrogen ionization zones in these regions. They also considered the effect of local He settling, and concluded it is not the primary process responsible for the high-frequency pulsation. Nevertheless, their model finds He to be deficient in the observable atmosphere at the magnetic poles. While He is not directly observable at visible wavelengths at the effective temperatures of the roAp stars ($6600 \leq T_{\rm eff} \leq 8200$ K), its gravitational settling implies that the magnetic poles are hydrogen-rich. We return to this point in Section 3.2 where we show evidence to support it.

Statistical studies of the roAp stars can be intriguing and informative, e.g. in the comparison of the roAp and noAp stars by Hubrig et al. (2000). But with only 40 such stars known, the class characteristics are still not well defined. Therefore, the greatest progress at present is to be made by in-depth studies of individual roAp stars, such as that for HR 3831 (e.g. Kurtz et al. 1997; Kochukhov 2006) and HR 1217 (Kurtz et al. 2005; Ryabchikova et al. 2007).

This is reminiscent of the related problem in the pulsational studies of δ Sct stars. Despite being the most abundant type of variable star, the major breakthroughs have been obtained through individual studies such as that of FG Vir (Breger et al. 2005). For the δ Sct stars, as for the roAp stars, the question of when pulsation modes are exited or not remains unanswered for physically similar stars – why do only some of these stars pulsate and what is the underlying physics? The many null results among roAp candidate stars strongly suggest that either the pulsation properties are not fully known (i.e. amplitude ranges or pulsation geometry) or the selection of candidates is too coarse. Individual studies of known roAp stars are therefore important (presently the only option at hand) to study the roAp properties in detail. Some examples of enlightening studies include that of γ Equ that clearly demonstrated the trends for pulsational amplitude with vertical stratification of chemical elements (Savanov, Malanushenko & Ryabchikova 1999; Kochukhov & Ryabchikova 2001), Doppler imaging of HR 3831 (Kochukhov 2004, 2006), and the study of line bisector variability by Kurtz, Elkin & Mathys (2006c) and a new type of upper atmospheric pulsation (Kurtz et al. 2006a, 2007).

1.3 The roAp pulsations

To first order, pulsations in many roAp stars are oblique axisymmetric dipole ($l = 1$, $m = 0$) p modes. Nevertheless, it has been clear for decades that normal modes described by single spherical harmonics are insufficient to explain fully the mode geometry in these stars. Uniquely, the oblique modes of the roAp stars allow them to be viewed from varying aspect, giving detailed information about the mode geometry. An early example was the study of HR 1217 by Kurtz et al. (1989) who showed the presence of alternating even and odd degree p modes, with the odd modes being consistent with oblique dipole modes, and the even modes not being consistent with either radial or quadrupole modes. This was confirmed by the more extensive Whole Earth Telescope study of this star by Kurtz et al. (2005). Even for roAp stars with single pulsation modes, in the best-observed cases – such as HR 3831 – it can be shown that the single mode is a distorted oblique dipole mode (Kurtz et al. 1997; Kochukhov 2006).

Any deviation from spherical symmetry for a pulsating star will give rise to distorted modes. For the roAp stars the dominant effect is the magnetic field, with contributions from the non-uniform abundance distributions and stellar rotation. The non-uniform abundance distributions are particularly important for spectroscopic studies – such as the one in this paper on HD 99563, and that of Kochukhov (2006) for HR 3831 – where concentrations of ions in spots mean that the pulsation mode is non-uniformly sampled with the rotation. However, photometric studies that more uniformly sample the mode geometry with rotation also show the distortions of the modes.

The effects of the magnetic field on the oscillations of roAp stars have been extensively studied theoretically, and there are

ongoing investigations into this complex problem (Dziembowski & Goode 1996; Bigot et al. 2000; Cunha & Gough 2000; Bigot & Dziembowski 2002; Saio & Gautschy 2004; Saio 2005; Cunha 2006; Sousa & Cunha 2008). While generally the magnetic field effect on the oscillations is expected to be small, the theoretical results do lead to expectations of distorted modes. For example, Saio & Gautschy (2004) studied the influence of the magnetic field on the pulsation geometry and found that not only can a dipole magnetic field explain the suppression of the observationally absent δ Sct modes, but it also leads to insufficiency of a single spherical harmonic to describe the pulsations angular dependency; a series of spherical harmonics of different degrees l are required. Inclusion of magnetic fields in the study and interpretation of roAp pulsations is therefore necessary and constitutes 'a formidable mathematical problem' (Saio & Gautschy 2004).

Saio (2005) continued the study of the effects of a dipole magnetic field on roAp pulsations and showed again that the field stabilized low-order p modes (such as those excited in δ Sct stars) for fields stronger than 1 kG, but that non-radial, high-order distorted dipole, or quadrupole, p modes remain overstable and are most likely to be excited in roAp stars. This is in excellent agreement with the current observations, as well as with the mounting observational and theoretical evidence for observable pulsation nodes in and above the photosphere in the magneto-acoustic layer. Further, and most interestingly, Saio modelled the latitudinal amplitude dependence for the roAp case of HR 3831 and found reasonable agreement with the observations by Kochukhov (2004).

Saio's non-adiabatic analysis predicts (his fig. 10) a latitudinal dependence of amplitude that does not differ from a purely dipole mode photometrically, whereas spectroscopy's ability to distinguish potentially between horizontal and radial pulsation components may detect the relatively smaller horizontal component when studying stellar spots close to (but not necessarily at) the magnetic poles. Saio's fig. 10 demonstrates a reasonable agreement with observed latitudinal velocity amplitude variation for HR 3831, but predicts higher amplitude towards the magnetic axis than is observed. However, the formation layer of the Nd lines used by Kochukhov in his observations is far above the boundary of Saio's models. Kochukhov (2006) also did not take into account the inhomogeneous Nd surface distribution.

The oblique pulsator model describes how non-radial pulsation modes seen from varying aspect with the stellar rotation show amplitude and phase modulation (see the overview by Kurtz & Martinez 2000) that results in a frequency multiplet in an amplitude spectrum, centred on the pulsation frequency ν and separated by *exactly* the rotation frequency $\nu_{\rm rot}$. This exact splitting by the rotation frequency allowed Kurtz (1982; see also Kurtz & Martinez 2000) to rule out the possibility that the observed multiplets can be explained by rotationally perturbed m modes (m being the azimuthal order of a mode), which is the typical interpretation of frequency splitting observed in other (non-oblique) non-radially oscillating stars, as such rotational multiplets are split by $(1 - C_{nl})\Omega$, where Ω is the rotation frequency, C_{nl} is a small constant dependent on the stellar structure, n is the overtone of the mode and l is its degree.

For oblique pulsation, the amplitude ratio of the multiplet components contains information about the pulsation geometry (assumed to be aligned with the magnetic geometry). In the case of a simple oblique dipole mode $(A_{+1} + A_{-1})/A_0 = \tan i \tan \beta$, where i is the inclination angle of the rotation axis, β is the obliquity of the pulsation/magnetic axis relative to the rotation axis, and A_0, A_{+1}, A_{-1} are the observed amplitudes of the frequency triplet. For modes that are not purely dipolar, or vary in structure with atmospheric depth in the stratified roAp stars atmospheres, this constraint can depend on the atmospheric depth of formation of the spectral lines studied (see e.g. Kochukhov 2006).

Despite the complex nature of roAp pulsations in the presence of magnetic fields and an oblique geometry, the observational data have rich potential for asteroseismic inference. Photometrically, multisite and space-borne observations allow the resolution of both the large and small frequency spacings and through them constrain the stellar dimensions and the interaction of the magnetic field and rotation with the pulsation modes. High-resolution time series spectroscopy allows the study of the pulsation geometry over the stellar surface (through line profile variability) and also vertically in the stellar atmosphere, through radial velocity measurements at different line bisectors, or through lines of elements located at different depths in the stratified atmosphere (e.g. Kurtz et al. 2006c; Ryabchikova et al. 2007). It is clear that the observations have begun to resolve the magneto-acoustic nature of the pulsations in these stars high into the atmosphere to levels that are unobservable in any other star but the Sun. Radial nodes are resolved in some stars such as HD 137949 (Mkrtichian, Hatzes & Kanaan 2003; Kurtz, Elkin & Mathys 2005c) and possibly HD 99563 (Elkin, Kurtz & Mathys 2005). Observed variation of pulsation phase with atmospheric depth shows the presence of running waves, and there is even an indication that shock waves are observed in the upper atmosphere of γ Equ (Shibahashi et al. 2008), and by inference other roAp stars with similar line profile variations.

1.4 HD 99563

HD 99563 was discovered to be a roAp star by Dorokhova & Dorokhov (1998), pulsating in a 10.70-min mode. It is a visual binary with a 1.2 mag fainter secondary at 1.79 arcsec separation (Fabricius & Makarov 2000). A spectroscopic study by Elkin et al. (2005) confirmed the monoperiodic pulsation found from photometry, and found the pulsations to have extremely high radial velocity amplitudes for a roAp star, such as 2.6 km s^{-1} for Hα and up to 5 km s^{-1} for Eu and Tm. For sake of clarity, we emphasize that *monoperiodic* refers to a single (physical) pulsation mode, e.g. the frequency quintuplet detected by Handler et al. (2006) (actually five components of a frequency septuplet) are all associated with only a single mode with pulsation frequency ν; the rest of the quintuplet describes the amplitude and phase modulation of the mode.

Elkin et al. (2005) measured a projected rotation velocity of $v \sin i = 28.5 \pm 1.1$ km s^{-1} from a high-resolution spectrum, while from narrow-band Strömgren photometric indices they estimated $T_{\rm eff} = 7700$ K and $\log g = 4.2$ (cgs). Furthermore, they studied variations in amplitude and phase for line bisectors, and from element to element. The demonstrably high amplitudes [and thus high signal-to-noise ratio (S/N)] and rich and varied information content from using lines of different elements or with line depth show HD 99563 to be a particular interesting roAp star for detailed study.

Handler et al. (2006) carried out a photometric multisite campaign and found an equally spaced frequency quintuplet in HD 99563, for the pulsation frequency $\nu = 1.5576539 \pm 0.0000007$ mHz. They determined the rotation period to be $P_{\rm rot} = 2.91179 \pm 0.00007$ d and a time of pulsation amplitude maximum to be HJD 245 2031.296 27. The photometry showed, through application of the axisymmetric spherical harmonic decomposition method of Kurtz (1992), that the mode of HD 99563 is dominated by a dipole component, with some contribution of an $l = 3$ component (i.e. the mode is a distorted dipole).

Handler and collaborators combined photometry, a *Hipparcos* trigonometric parallax and the temperature and surface gravity estimate by Elkin et al. (2005) to constrain the basic parameters of HD 99563. Under the assumption that the secondary star in the visual binary is a physical binary component and that the wide orbit indicates the stars have evolved separately, the estimated parameters of both stars must fit two stellar evolutionary models of the same age. By adopting $T_{\rm eff} = 7900 \pm 300$ K and $\log g = 4.152$, they found for the primary $\log L/L_\odot = 2.03$, $R/R_\odot = 2.38$, an inclination angle of the stellar rotation axis $i = 43\overset{\circ}{.}6 \pm 2\overset{\circ}{.}1$ and a magnetic obliquity $\beta = 86\overset{\circ}{.}4 \pm 0\overset{\circ}{.}3$. This makes HD 99563 especially interesting because of its high pulsation amplitude, its rotation that is fast enough for Doppler imaging and its (for a roAp star) rare favourable orientation where both magnetic poles become visible throughout a rotation cycle.

Hubrig et al. (2004) were the first to measure the magnetic field of HD 99563, finding a longitudinal field of -688 ± 145 G on HJD 245 2494.483, or rotation phase 0.08 with respect to Handler et al.'s pulsation ephemeris. Hubrig et al. (2006) published another two measurements at rotation phases 0.07 and 0.09 showing -235 ± 73 and 670 ± 37 G, respectively. Further, using the Russian 6-m telescope at the Special Astrophysical Observatory of the Russian Academy of Sciences (SAORAS), Elkin et al. (2008b) obtained six additional magnetic longitudinal field measurements near rotation phases 0.25, 0.5 and 0.75. With all nine available measurements, these authors used the well-known relation for a dipolar magnetic field

$$B_{\rm l} \propto B_{\rm p} \cos\alpha, \tag{1}$$

where

$$\cos\alpha = \cos i \cos\beta + \sin i \sin\beta \cos\Omega t, \tag{2}$$

α is the angle between the magnetic pole and the line-of-sight, i is the rotational inclination, β is the angle between the rotation axis and the magnetic axis, Ω is the rotation frequency, $B_{\rm l}$ is the longitudinal magnetic field strength and $B_{\rm p}$ is the polar field strength.

As can be seen from equation (2), the mean magnetic field strength $\langle B_{\rm l}\rangle \propto \cos i \cos\beta$ and the amplitude of the magnetic field variations $A_{B_{\rm l}} \propto \sin i \sin\beta$. Thus, $\tan i \tan\beta = A_{B_{\rm l}}/\langle B_{\rm l}\rangle$, from which β can be constrained when i is known. Using the measured values for HD 99563, $\langle B_{\rm l}\rangle = 21 \pm 58$ G and $A_{B_{\rm l}} = 701 \pm 114$ G, Elkin et al. (2008b) find an inclination of $i = 43\overset{\circ}{.}5$ and a magnetic obliquity $\beta = 88^\circ$ (84°–90° for a 1σ range), which are similar to those determined by Handler et al. (2006). The magnetic minimum coincides with the moment of maximum modulated pulsation amplitude ($\varphi_{\rm rot} = 0$ hereafter), and similarly for the maximum half a rotation phase later ($\varphi_{\rm rot} = 0.5$). This is consistent with both magnetic poles being viewed from a similar angle and coming into view for almost the same duration (requiring that either i or β be close to 90°), and with the pulsation axis and magnetic axis being aligned. As a matter of interest, an oblique, centred magnetic dipole has a polar magnetic field strength about 3.2 times the maximum longitudinal field strength measured (Preston 1967), implying a polar field strength for HD 99563 of ~2.3 kG.

Kochukhov (2004) used Doppler imaging to construct the first tomographic maps of pulsation velocity, surface abundance and magnetic field map for the roAp star HR 3831. With observations obtained over a wide range in rotation phase for HD 99563, it will be possible to do this with higher precision for this star because of its very high amplitudes, and it will be possible to look simultaneously at the additional dimension of the atmospheric depth dependence of the velocities. Kochukhov, as a first approximation, treated the analysis of HR 3831 as if the atmosphere has a single pulsation layer. Observations of HD 99563 and other roAp stars show the situation to be much more complex than this. Disentangling the vertical and horizontal pulsation characteristics is a challenge, but one with rich rewards for the fields of asteroseismology, pulsation theory, magnetohydrodynamics, stellar atmosphere theory and atomic diffusion.

HD 99563 is one of only a few known roAp cases where tomographic mapping through Doppler imaging is possible, based on rotation rate and the orientation of the magnetic field. Therefore, observations over three nights (most of the 2.91-d rotation period) were scheduled from two sites simultaneously – Subaru on Mauna Kea and VLT on Cerro Paranal – to attempt to collect spectra at high resolution in both time and dispersion to obtain a first picture of this star's photosphere, and to determine precisely its physical parameters. Theoretically, the scheduled observations would have given us 70 per cent coverage of the rotation cycle, hence of the visible stellar surface. But due to bad weather, only one site contributed significantly to the pulsation study, and only some 40 per cent rotational coverage was attained.

In this first of a series of papers on HD 99563, we are studying the horizontal pulsation geometry with the stellar rotation. A Doppler imaging study of the surface abundance distribution of many ions and detailed modelling of the horizontal and vertical pulsation geometry are in preparation.

2 OBSERVATIONS AND DATA REDUCTION

Time series spectroscopy observations were collected on Cerro Paranal with the VLT UV-Visual Echelle Spectrograph (UVES) during three nights in 2007 March; a journal of observations is given in Table 1. UVES is an echelle spectrograph and we used the settings for the wavelength range 4970–7010 Å (with a 60-Å wide gap near 6000 Å) at $R = 110\,000$. The UVES instrument was used with an image slicer and a 0.3 arcsec slit. Typical exposure times were 40 and 65 s, and 80 s at high airmass on the second night. With ~26 s readout and overhead time, a time resolution of 66–106 s was obtained.

Table 1 lists the spectra collected each night. With the 2.91-d rotation period of HD 99563, the three-night run was scheduled to cover most of a rotation cycle of HD 99563 (rotational phases 0.02–0.84) and was coordinated with a run using the High Dispersion Spectrograph (HDS) on the 8.2-m Subaru Telescope at Mauna Kea to obtain the rotational phases coinciding with daytime on Paranal. However, humid weather conditions at Mauna Kea resulted in only 35 sporadic observations that are not included in the frequency analysis in Section 3.1, but were instead combined into two average spectra at rotation phases 0.23 and 0.56 and used in Doppler imaging to produce surface maps for chemical elements, only two of which are shown in this paper (see Figs 8 and 13 below); a full Doppler imaging analysis will be presented in a future publication.

Our new Doppler imaging code, called IA, is a modification of the previously developed code, known as PCI, described in Savanov & Strassmeier (2005). Instead of temperature inhomogeneities on the surfaces of cool stars, our new code inverts the time series of spectral line profiles into surface maps of chemical abundances. IA uses interpolation in precalculated local intrinsic synthetic spectra organized as lookup tables. These synthetic spectra are calculated for a set of abundances ε for given parameters of the investigated star: $T_{\rm eff}$, $\log g$ and microturbulence ξ. Other input parameters are the equatorial rotational velocity, inclination of the rotation axis i and the instrumental profile. The code uses Tikhonov regularization

Table 1. Journal of VLT observations indicating nightly observing date (UT), rotation phase with reference to a time of spectroscopic pulsation maximum, HJD 245 4171.43328, Heliocentric Julian Date (HJD) range, typical exposure time, number of collected spectra and mean S/N. The S/N ratios are based on the random noise in the continuum of consecutive spectra, or for single spectra based on predicted ratios. The 2004 data were re-reduced in same manner as the new data, and included in the analysis as they supplement the covered rotation phases. An additional 35 spectra were obtained with the HDS at the Subaru Telescope on 2007 March 12 and March 13 and combined into two average spectra at rotation phases $\varphi_{\rm rot} = 0.23$ and 0.56.

Date (UT)	Rotation phase $\varphi_{\rm rot}$	HJD range (−245 0000)	$t_{\rm exp}$ (s)	n	S/N λ5100	S/N λ6400
2004 March 06	0.937–0.966	3070.60–3070.69	40	111	120	95
2007 March 12	0.021–0.150	4171.53–4171.91	40	518	75	55
2007 March 13	0.365–0.494	4172.52–4172.90	40/80	417	85	60
2007 March 14	0.708–0.837	4173.52–4173.90	65	372	110	75

and minimizes the expression

$$E(\varepsilon) = \sum_{\lambda} \left(I^{\rm obs}_{\lambda\varphi} - I^{\rm calc}_{\lambda\varphi}(\varepsilon)\right)^2 / \sigma_{\lambda\varphi} + \Lambda F(\varepsilon), \quad (3)$$

where $I^{\rm obs}_{\lambda\varphi}$ and $I^{\rm calc}_{\lambda\varphi}$ represent the observed spectra and calculated line profiles for a given surface abundance distribution ε. The position of the elementary pixels on the stellar surface is specified by latitude and longitude φ and λ. The difference between observed and theoretical spectra is weighted by the individual errors of measurements $\sigma_{\lambda\varphi}$. F(ε) is the Tikhonov regularization function

$$F(\varepsilon) = \sum_{i} || \nabla\varepsilon_i ||^2, \quad (4)$$

which provides a measure of the smoothness of the surface distribution ε, and Λ is a regularization parameter (the index i runs over all surface elements). For further details on the Doppler imaging programme and production of the tomographic maps, see Savanov & Strassmeier (2005).

The spectra were reduced to 1D with the pipelines provided by ESO with the standard calibration data (bias, flat-field and Thorium-Argon wavelength reference spectra). The S/N was 27 per cent lower than predicted with ESO's online exposure time estimation tool. The observing conditions were in general good, all three nights were clear and dry, with typical seeing of 0.5–0.8 arcsec, except for the first night where seeing was 0.7–1.1 arcsec during the first half of the night and then deteriorated to 0.8–2.4 arcsec thereafter.

Special effort was therefore made to optimize the reduction. We used the UVES PIPELINE 2.9.7 (based on MIDAS) and applied minor additional corrections. We smoothed out a CCD bias pattern for every 3.5 columns (RED upper CCD), inserted two columns missed during CCD readout (with minor effects on the 2D wavelength calibration) and fixed the rebinning step sizes of the 1D spectra to 0.01787 Å (RED upper CCD) and 0.01526 Å (RED lower CCD). To eliminate wavelength drifts, wavelength calibrations were made to the nearest Th-Ar reference spectrum (obtained every 3 h).

Continuum rectification of the 1D spectra was performed iteratively: individual spectra were normalized to a run master from the most stable night (starting on 2007 March 12) using a fourth-order polynomial, then these were normalized to master spectra of individual nights. After inspection, subsets of the resulting spectra were corrected for remaining slopes. The nightly masters were rectified through iterative normalization using spline fitting to pseudo-continuum windows identified from comparison to a model spectrum. Features due to cosmic rays and blemishes were removed with a semi-automatic cutting procedure. Barycentric corrections, which changed by about 1.0 km s^{-1} over a single night, were registered and applied in the period analysis, but not in the wavelength calibration and final rebinned 1D spectra.

Table 1 gives the estimated S/N of the spectra based on random noise measured in difference spectra of pair-wise subsequent spectra. Because the 2007 data had 27 per cent lower S/N than predicted, and also compared to the 2004 observations for the same exposure time, exposure times were increased to 60 s most of the two last nights in 2007. This difference is not due to weather, as large seeing variations are found to have only small influence on the S/N (as a consequence of the image slicer). Comparing the 2D spectra of the 2 yr confirms that fewer photons were collected in 2007 than in 2004. About 10 per cent variation in S/N is due to the differences in airmass, since in 2007 we observed HD 99563 during full nights. Part of the reason for the lower S/N is from centring of the slicer on the object, but alone this cannot explain the loss. The spectra from the upper CCD, redward of 6000 Å, show a systematic noise pattern of undulations with ∼3.4 cycles per Å, for stretches of ∼30 Å occurring every ∼67 Å, starting at 6070 Å. This coincides with the first half of each Echelle order. As HD 99563 rotates relatively quickly, resulting in broad lines, we smoothed 1D spectra of the upper CCD over 3–4 pixel, which strongly suppressed the artefact pattern. Comparing our frequency analyses for lines from the lower and upper spectra gave no significant differences. We suspect the origin of this feature is a sort of amplification of the aforementioned 3.5 column pattern at the order merging regions. During the last night, a 1-h gap in the time series occurred when the image acquisition system failed to save the observations.

3 DATA ANALYSIS AND RESULTS

3.1 Line analysis

For the purpose of spectral line identification, a synthetic comparison spectrum was produced with SYNTH (Piskunov 1992) using a Kurucz stellar atmosphere model. Atomic line data were taken from the Vienna Atomic Line Data base (VALD; Kupka et al. 1999) for ions with increased abundances, mainly for Nd, Pr, Sr, Cr and Eu. Other sources used for line data were the atomic data base NIST (National Institute of Standards and Technology)[1] and the Data base

[1] http://physics.nist.gov

on Rare Earth Elements at Mons University (DREAM;[2] Biémont, Palmeri & Quinet 1999) through its implementation in the VALD. The line selection and line analysis is fully based on lines identified in table 1 of Elkin et al. (2005).

3.1.1 *Radial velocity shifts*

Because of the non-uniform surface distributions and stratification of ions in the atmospheres of Ap stars, high-overtone mode pulsation amplitude and phase vary from element to element, and even within individual lines as a function of line depth (atmospheric height). Line profiles are variable because of non-radial pulsation, non-uniform abundance of elements over the surface because of spots and non-uniform abundance with depth because of stratification. It is our intention with this and future studies of the data presented here to disentangle these contributions to extract 3D radial velocity maps of the stellar pulsation geometry.

IDL tools for line measurements and analyses were used as described in Freyhammer et al. (2008a). Precise radial velocity shifts were measured for many spectral lines with the centre-of-gravity (CoG) method and by fitting with Gaussian profiles. We made our measurements with respect to the continuum – normalized to unity – in the selected regions of the measured lines, which gave smaller amplitudes for the CoG procedure. This method, however, was preferred for pulsation studies because of its better ability to deal with blended line profiles. For strong and isolated lines, the two methods were comparable. However, in some cases Gaussian fitting was used in automated measurements as it is more stable when the whole line profile shifts considerably due to, e.g. rotational mean radial velocity modulation (see Section 3.2) when one of the line wings goes outside the pre-defined wavelength window. The main difference of the two methods is their estimates of pulsation amplitudes. The CoG method is very sensitive to continuum placement and more sensitive to subtle, intrinsic line profile variations of relatively weak, asymmetric lines.

The radial velocity measurements were automated with a wavelength window defined for each line in a high S/N average spectrum. That window was shifted in wavelength to account for the barycentric correction for each individual spectrum, then the profile was fitted with both a Gaussian and by CoG fitting; finally, barycentric corrections were added to the resulting radial velocities. The two radial velocity series were then compared.

Because of the occurrence of substructure in absorption features of elements with inhomogeneous surface distributions, we used two approaches to study line variability: (1) to study an element's integrated radial velocity behaviour, we used the full line profile, whereas (2) for line profiles with subfeatures caused by inhomogeneous (spotted) surface distributions, we measured each substructure in a line and followed it over the half a rotation cycle for which it was visible. The line windows for the 'spot' features (two for Nd and three for Eu; see below in the text and Figs 10 and 14 for clarification) were defined in 1-h subseries of spectra (for a total of 32 time bins), rather than one window for all 1418 spectra. The former approach was useful for fitting multiplet terms (Section 3.2), while the latter approach was particularly useful for studying pulsation amplitude and phase variations with rotation phase.

[2] http://w3.umh.ac.be/~astro/dream.shtml

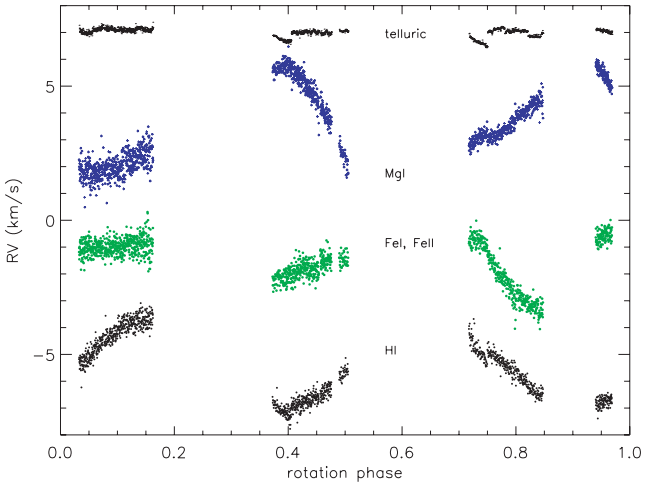

Figure 1. Rotational radial velocity trends for different elements: telluric lines (2 lines combined), Mg (two Mg I lines combined), Fe (combined from 4 Fe I and Fe II lines), and the hydrogen core (prewhitened for pulsations). Barycentric corrections were applied to the radial velocities of stellar lines and are relative to those of the telluric lines. Radial velocity offsets were added to each series' ordinates for clarity. If the radial velocity variation with the rotation period were the result of reflex motion of HD 99563 in a binary orbit with an unseen close companion, the amplitudes and trends of relatively homogeneously distributed elements, such as iron and hydrogen, should be the same; they are not. The radial velocities for the iron measurements that deviate most from those for Hα at phase 0.94 are from 2004, but there is also significant deviation at phases 0.02–0.17 in the 2007 data. Mg shows significantly different trends from Fe and H, but this is most probably caused by a patchy surface distribution. Because of the non-uniform abundance distributions, orbital radial velocity shifts of HD 99563 can only be ruled out for amplitudes significantly larger than those seen here.

3.1.2 *Frequency analyses*

Frequency analyses were performed using a Discrete Fourier Transform programme (Kurtz 1985) and the PERIOD04 (Lenz & Breger 2005) programme. The former fits cosines while the latter uses sines, so all phases determined with PERIOD04 were recalculated to match the cosine fitting in units of radians. The noise, σ, of fitted amplitudes and phases (see e.g. Tables 2 and 4) was determined from least-squares fitting to the data following Deeming (1975); it is the standard deviation of one measurement with respect to the fitted function.

Trends in the radial velocities with the rotation were strong for all lines, even Hα and Fe (Fig. 1), indicating that HD 99563 is very spotted. Linear and non-linear trends were fitted and removed with linear or polynomial least-squares fitting, and in a few cases also by prewhitening low-frequency peaks from the radial velocity series. The origin of these trends is discussed further in Section 3.2, but most of the contributions are stellar; with the 0.3-arcsec slit, no image slicer and seeing conditions of 0.9–1.4 arcsec, the centring error for UVES is only 50–100 ms^{-1} (Bouchy et al. 2004). Furthermore, a 1-mbar change in pressure may induce drifts of 90 ms^{-1}. Therefore, instrumental shifts were less than $\sim$300 ms^{-1} per night, depending on seeing and pressure.

The telluric lines in Fig. 1 show that the wavelength calibration sometimes has small offsets (up to 600 ms^{-1}) between reductions using different wavelength reference spectra. These are artefacts from not interpolating over all reference spectra for a night, an option not available with the UVES pipeline, and then rebinning to same-width wavelength bins. However, as the time-scale of these

Table 2. Amplitudes and phases determined from a least-squares fit of the listed frequencies to the Hα radial velocity series. Column 3 gives the frequencies calculated relative to a value of ν slightly revised from that of (Handler et al. 2006) (to tie together the 2004 and 2007 data sets) and to $\nu_{\rm rot}$. The frequency nonuplet was required to have components separated by exactly the rotation frequency. A 2 c d^{-1} low-frequency periodicity that is believed to be an artefact was removed. Errors on ν and $\nu_{\rm rot}$ from (Handler et al. 2006) are $\sigma_\nu = 0.000007$ mHz and $\sigma_{\nu_{\rm rot}} = 0.0000001$ mHz. Prewhitening for this solution leaves point-to-point scatter in the residuals of 212 ms^{-1}. Gaussian fitting to the profile was used. The zero-point for the time-scale, t_0 = HJD 245 4171.43328, was selected so that the phases of $\nu - \nu_{\rm rot}$ and $\nu + \nu_{\rm rot}$ are equal; i.e. this is the time of pulsation amplitude maximum, as given in equation (6).

Id.	Freq. (mHz)	Freq.(rev.) (mHz)	Amplitude (ms^{-1})	Phase (rad)	S/N
ν	1.5576530	1.5576482	156 ± 31	-2.56 ± 0.20	5.1
$\nu - \nu_{\rm rot}$	1.5536779	1.5536733	1726 ± 32	-2.17 ± 0.02	54.3
$\nu + \nu_{\rm rot}$	1.5616281	1.5616231	1303 ± 32	-2.18 ± 0.02	41.0
$\nu - 2\nu_{\rm rot}$		1.5496984	121 ± 22	-2.11 ± 0.18	5.5
$\nu + 2\nu_{\rm rot}$		1.5655980	80 ± 22	0.42 ± 0.27	3.7
$\nu - 3\nu_{\rm rot}$	1.5457276	1.5457235	449 ± 20	-2.63 ± 0.04	22.2
$\nu + 3\nu_{\rm rot}$	1.5695784	1.5695729	105 ± 20	1.25 ± 0.19	5.3
$\nu - 4\nu_{\rm rot}$		1.5417486	35 ± 19	1.56 ± 0.55	1.8
$\nu + 4\nu_{\rm rot}$		1.5735478	123 ± 19	-1.87 ± 0.16	6.4
2ν	3.1153060	3.1152963	129 ± 8	0.95 ± 0.06	15.9
$\nu_{\rm rot}$	0.0039749		53 ± 11	-3.14 ± 0.26	4.9
$2\nu_{\rm rot}$	0.0079498		1600 ± 13	-1.90 ± 0.01	127.0
$2\nu - 2\nu_{\rm rot}$	3.1073557	3.1073465	72 ± 8	0.48 ± 0.11	8.8

offsets is very different from that of the pulsations (3 h as opposed to 11 min), we did not correct this in the analysis. Telluric lines only provide accurate and precise velocity references within a few hundred ms^{-1}, as they are influenced by fast and changing wind speeds in the high layers of the Earth's atmosphere where they are formed.

3.2 Hydrogen core

Handler et al. (2006) detected 10 frequencies in their time series multisite campaign *B*-band photometry of HD 99563. These are comprised of (Table 2) the pulsation frequency $\nu = 1.557653 \pm 0.000007$ mHz, the rotational split oblique dipole frequency quintuplet $\nu \pm \nu_{\rm rot}$ and $\nu \pm 3\nu_{\rm rot}$, and other harmonics or combination frequencies. These authors identified the rotation frequency as $\nu_{\rm rot} = 0.0039751$ mHz and gave the photometric ephemeris (in days) with respect to the time of photometric modulated pulsation amplitude maximum as

$$t(\max) = \text{HJD}\,245\,2031.296\,27 + 2.91179 \pm 0.00007\,E, \qquad (5)$$

where t(max) gives the time in HJD corresponding to the given number of epochs E elapsed since the reference point in time. The decimal part of E corresponds to the rotation phase in the case of HD 99563. The pulsation frequency ν itself has the second lowest amplitude of the quintuplet. See Handler et al.'s fig. 5 for a schematic view of their frequency quintuplet.

The Hα-core line-forming region extends over a considerable vertical region of the chemically stratified photosphere, in contrast to other elements. Radial velocity measurements of this line therefore compare well to the photometry, and as Hα for this star has a high pulsation amplitude in excess of 2 km s^{-1}, we used this line for the initial frequency analysis. Because of the limited accuracy of the rotational period in equation (5), a reference epoch close to our 2007 observations was chosen at the moment of maximum of the modulated pulsation amplitude of Hα:

$$t(\max) = \text{HJD}\,245\,4171.43328 + 2.91179\,(\pm 0.00007)\,E, \qquad (6)$$

while the value of the pulsation frequency ν by Handler et al. (2006) was revised within its error to $\nu = 1.5576530$ mHz in order to tie the new spectra together with the 2004 data set (see Section 3.2.1).

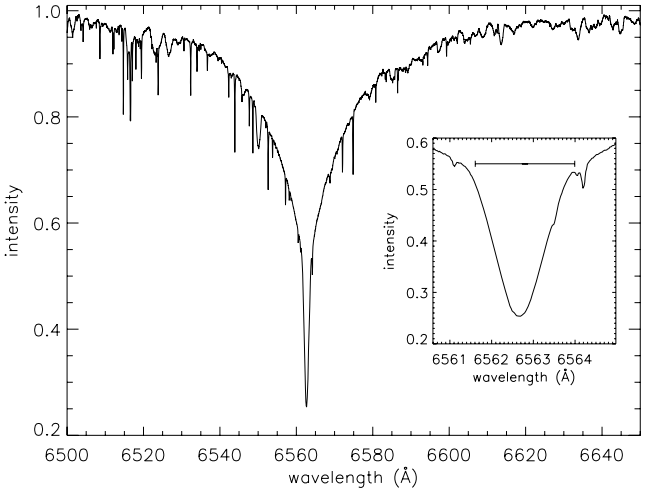

Figure 2. Average spectrum of the Hα region. The insert shows the line core, with the region measured for radial velocities marked with a bar.

3.2.1 *Trends of the radial velocity shifts*

The Hα profile is shown in Fig. 2. The insert shows the line core, with the region measured indicated with a bar. Radial velocities, measured through Gaussian fitting to the line profile cores, are shown in Fig. 3, phased with the rotation period. These reveal a

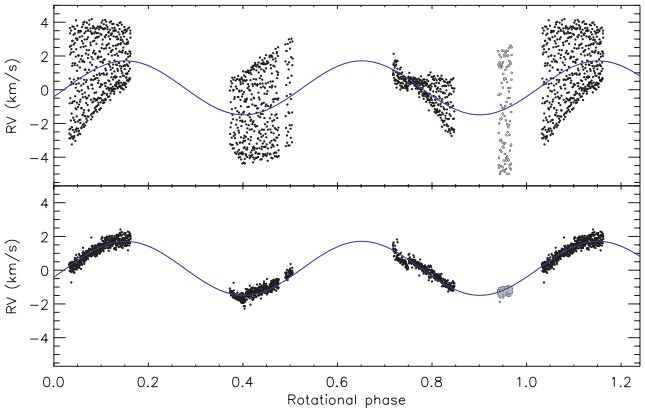

Figure 3. Radial velocities for HD 99563 measured in the line core of Hα for the 2007 observations (black dots) and the 2004 data (grey dots at phase 0.94). The modulated pulsation amplitude is superposed on a rotational modulation of the average radial velocity (fitted with solid line). Rotation phases are relative to equation (6). The top panel shows measured radial velocities, while the bottom panel shows rotational radial velocities that remain after removing the pulsational variations by prewhitening the *pulsation* frequencies (i.e. the pulsational frequency nonuplet) in Table 2. The broad-band of data in the top panel is not caused by scatter; it is the pulsation compressed in time. Fig. 5 shows these data expanded in time where the pulsation cycles can be seen.

double wave sinusoidal variability of the *average* radial velocities with an amplitude of 1.6 km s^{-1} and with a frequency twice that of the rotation frequency, $2\nu_{\rm rot} = 0.0079498$ mHz. Using the frequency analysis tool PERIOD04 (Lenz & Breger 2005) to improve phases and amplitudes iteratively for the solution of Handler et al. (2006) (for fixed frequencies, keeping only the significant ones), the $2\nu_{\rm rot}$ modulation is found (Table 2) to have an amplitude of 1600 ms^{-1}. Single or double wave angular modulation of the mean radial velocity of stars is known from many other elements in spotted stars – particularly the rare earth elements – but has not previously been detected for hydrogen.

Comparison with telluric lines, constant within 600 ms^{-1}, excludes a non-stellar origin (Fig. 1) for the Hα rotational radial velocity variations. Detailed comparison of averaged spectra in bins of 35 min show the slow periodicity in Fig. 1 dominates in the blue wing and central part of the slightly asymmetric Hα core. A blend with a line of a rare earth element distributed mainly around the stellar poles cannot be completely excluded as the source of the radial velocity curve. However, we consider it unlikely, based on comparison to a synthetic spectrum, that such relatively weak lines (compared to the Hα core) can result in the amplitude observed.

The variation in the mean radial velocity of the Hα line with rotation is shown in Fig. 3, with the pulsation variation present (in the top panel) and after prewhitening for the pulsational nonuplet (given in Table 2). There are several possible explanations for this rotational variation that we now examine.

3.2.2 *Variations in the mean radial velocity caused by line profile variations*

We modelled line profile variations for an oblique dipole pulsation mode with a rotational inclination of $i = 44^\circ$, pulsation pole obliquity of $\beta = 88^\circ$, an equatorial rotational velocity of 30 km s^{-1} and a pulsational amplitude of 14 km s^{-1} – values appropriate for HD 99563. The synthetic line profiles were computed using an adapted version of the line profile code implemented in FAMIAS (Zima 2006, 2008). The underlying model approximates the velocity field by a spherical harmonic, assumes a Gaussian intrinsic profile that originates from a 2D atmospheric layer and is weighted with a fourth-order limb darkening law. We adapted the above-mentioned code to include the effects of oblique pulsation on the line profile variations.

We computed a first set of synthetic line profiles for a complete rotation cycle, assuming uniform element distribution across the stellar surface. We then measured the radial velocities for the model data by computing the first moment of the line profile. The top panel of Fig. 4 shows that in this case the radial velocity amplitude is modulated whereas the rotational variation of the mean radial velocity of the model line is negligible. Therefore, the radial velocity variation with the rotation period for Hα is not a consequence of line profile variations for a simple oblique dipolar pulsation mode.

3.2.3 *An unseen binary companion in a synchronous orbit*

An obvious possible explanation for the radial velocity modulation seen in Fig. 3 is to hypothesize an unseen binary companion. In this case, the orbital period must be equal to the rotation period of HD 99563, and that is reasonable for a 2.91-d rotation period as synchronism is expected for such a short orbital period. There is no secondary spectrum seen, thus the single-lined spectroscopic binary mass function is

$$\frac{(m_2 \sin i)^3}{(m_1 + m_2)^2} = (v_1 \sin i)^3 \frac{P}{2\pi G} = 1.24 \times 10^{-6}\ {\rm M}_\odot, \qquad (7)$$

where the primary's projected orbital velocity $v_1 \sin i = 1600$ m s^{-1} is from Table 2. The component masses m_1 and m_2 are for the primary (pulsating) component and the less massive secondary component respectively and P is the orbital period (assumed to be identical to the primary's rotation period). Assuming the orbital plane is the same as HD 99563's equatorial plane – a reasonable assumption for such a close system – gives the orbital inclination i to be the same as the rotational inclination derived by Handler et al. (2006), $i = 44^\circ$. With this inclination, the very small mass function shows that

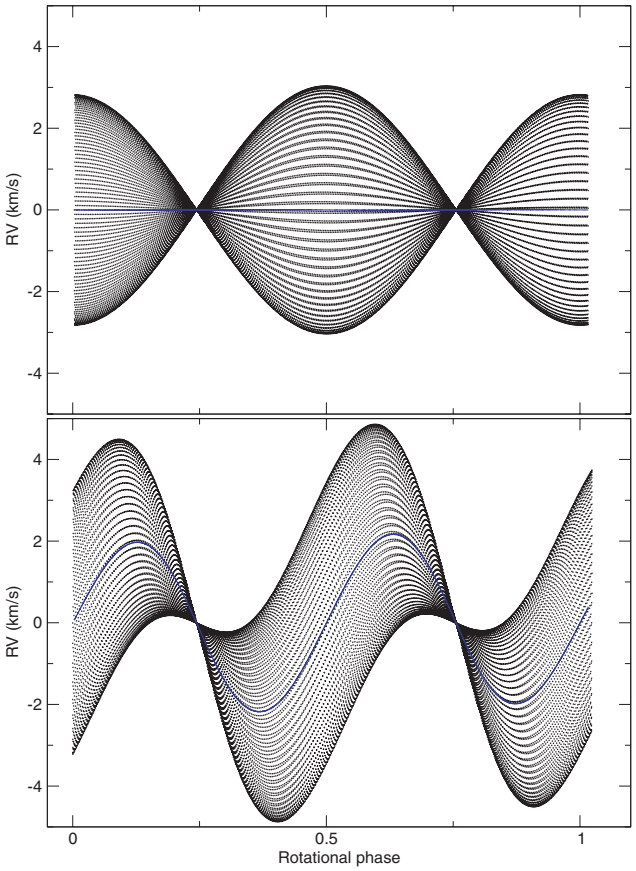

Figure 4. Top panel: radial velocities over the rotation period (black dots in electronic version) and its running mean (solid line at RV = 0 km s^{-1}) for model line profile variations of an oblique dipole pulsation mode and uniform element distribution with $i = 44^\circ$, $\beta = 86^\circ$, $v \sin i = 30$ km s^{-1} and a pulsation amplitude of 14 km s^{-1}. The radial velocity amplitude is modulated due to the changing aspect angle of the pulsation mode, whereas the mean shows no significant variation. The abscissa is rotation phase. Bottom panel: same as the top panel, but with a non-uniform element distribution that is higher near the magnetic poles, simulating H abundance spots. Both the radial velocity amplitude and its mean are modulated due to the stellar rotation in the same way as the observations of the Hα line. As for Fig. 3, the model data here are compressed in time so that the pulsations appear only as a broad-band. If this figure were expanded in time (as in Fig. 5 for the Hα data), then the pulsation cycles would be visible. The important features to be noted are the envelope of the data, which shows the amplitude modulation, and the mean radial velocity. Comparison of the lower panel with the Hα data in the upper panel of Fig. 3 shows the plausibility of our hypothesis that the variation in mean radial velocity is caused by enhanced hydrogen spots at the magnetic poles.

$m_1 \gg m_2$. Taking the mass of HD 99563 to be that estimated by Handler et al. (2006), $M = 2\,M_\odot$, gives $m_2 = 0.025\,M_\odot$, or about 26 Jupiter masses with a separation between the components of about $11\,R_\odot$.

Thus, one explanation of the radial velocity variation in Hα with rotation is a close, hot Jupiter companion in a synchronous orbit. The current exoplanet listing[3] indicates that this is not unreasonable when compared to other known exoplanets. This, if true, is an exciting result, as no planet has been discovered orbiting a magnetic Ap star.

If a planetary companion is the explanation for the Hα rotational radial velocity variation, then we expect all spectral lines to show the same radial velocity curve. Testing this for HD 99563 is complicated by the spotted nature of its atmosphere, causing all spectral lines to vary with rotation, but with different amplitudes and phases depending on the abundance distributions. For example, other elements, such as Mg in Fig. 1, show different mean radial velocity curves (also when using telluric lines as reference for the wavelength calibration), whereas in the same figure, Fe shows some similarities with Hα. Because the rotational radial velocity amplitudes of various elements caused by the spots are comparable to, or higher than, the rotational amplitude variation seen in Hα, a hot Jupiter remains a possible explanation, but not our preferred one.

3.2.4 *Spots of enhanced H at the magnetic poles*

We suggest this is the first detection of enriched H abundance spots near the magnetic poles, as is expected theoretically from helium depletion by gravitational settling (Balmforth et al. 2001). Such spots give rise to extra absorption superposed on the mean Hα core line profile that is variable with the rotation of the star. When a hydrogen spot is in the centre of the disc, the radial velocity contribution from its extra absorption is zero. Then, as it moves away from the centre the extra absorption is in the part of the disc that rotates away from us, giving rise to a redshift of the line. As the spot reaches the limb, the opposite spot is coming into view on the other side of the disc, increasingly cancelling out the redshift by a blueshift. At quadrature (or in this case, magnetic crossover), both spots cancel out the contribution to the mean profile and the radial velocity shift is zero. This is followed by a blueshift. This is what is seen in Fig. 3; the phasing is correct; the double wave is as expected.

To simulate the scenario of enriched element abundance spots near the magnetic poles, we followed the same procedure as in Section 3.2.2 above, but in this case with weighting of the local intrinsic line width W with respect to the latitude θ of the displacement field using the following arbitrary function

$$W(\theta) = W_0(1 + \cos^2\theta). \quad (8)$$

The resulting shape of the radial velocity curve is displayed in the bottom panel of Fig. 4. The radial velocity amplitude as well as its mean value are modulated with an amplitude that is comparable to the observations of the Hα line.

Thus, our hypothesis that the observed Hα line core's radial velocity variation with rotation is caused by theoretically expected hydrogen abundance spots is consistent with our simple model. Furthermore, and more importantly, we predict that if our hypothesis is correct, then hydrogen spots will be detectable with stellar rotation for other Ap stars with strong magnetic fields of similar configuration and orientation as HD 99563. We plan tests of this prediction.

Of course, even if hydrogen were uniformly distributed, there would be some rotation variation in its equivalent width as a result of the cooler spots at the magnetic poles caused by suppression of local convection by the vertical magnetic flux tubes and by the non-uniform distribution of other elements – primarily rare earth elements. However, in this case the contribution, if any, from the polar regions is a reduced absorption in the hydrogen lines (for stars cooler than A5-type stars), which would produce radial velocity variations in the opposite sense to our hydrogen spot explanation. This does not agree with what is seen in Fig. 3. In addition, the general shape and phase of the modulated mean radial velocity curve from hydrogen spots must match that of other elements concentrated near the stellar poles. Nd is such an example (see the Doppler imaging map in Fig. 8) and, except from different amplitude and that the lines become double at magnetic crossover, the phases of the modulation are similar (see Fig. 11).

3.2.5 *Detected frequencies*

The frequency resolution of our 2007 data alone, 4.8 μHz, is insufficient to improve the period by Handler et al. (2006). However, by revising the pulsation frequency ν in a test grid within the 1σ error given by Handler et al., we could also include the 2004 data in the fit. This revision was done by recalculating the first seven frequencies by Handler et al. (column 2 in Table 2) relatively to the values of the trial frequency ν, using fixed amplitudes. A small revision (+4.8 μHz) of ν, chosen as the closest alias to their value of ν, gave a good fit to the frequency quintuplet and residuals of only 245 ms^{-1} per observation for all 2004–07 data and 10 ms^{-1} for the highest peaks in amplitude spectrum of the residuals to the fit. The revised frequency is henceforth used as ν, but we emphasize that it is a convenient alias out of many choices that phases the 2004 data with the 2007 data, rather than an improvement in precision to the multisite result by Handler et al. (2006). We note that combining the two data sets cannot improve the frequency determination more than with the 2007 data alone, due to the introduction of several ambiguous aliases that are all good candidate frequencies. Yet, the 2004 data supplement the pulsation analysis at other rotation phases and were therefore usefully included.

After prewhitening the full radial velocity series (all 2004–07 data) for the mean radial velocity modulation (at $2\nu_{\mathrm{rot}}$) and the first seven significant frequencies in the solution by Handler et al. (2006), we detected excess power in the residuals. By including nine terms spaced equally in frequency by the rotation frequency, we found all but one to be significant; we refer to these nine frequencies as a nonuplet. Figs 3 and 5 show, respectively, the radial velocity series prewhitened for the nonuplet frequencies and for the rotational mean radial velocity modulation. The amplitude of hydrogen pulsational radial velocity variations ranges from a few hundred m s^{-1} to almost 4 km s^{-1}. Fig. 6 illustrates the nonuplet frequencies, while Table 2 (columns 4 and 5) gives the corresponding amplitudes and phases determined from a linear least-squares fit.

3.2.6 *Amplitude and phase variations*

Amplitude and phase variations were measured with radial velocities from Gaussian fits to the line core of Hα (Fig. 2) in 32 bins of about 1-h duration. The result is shown in Fig. 7. The superposed full line is for a rotationally modulated amplitude nonuplet pattern

[3] http://exoplanets.org

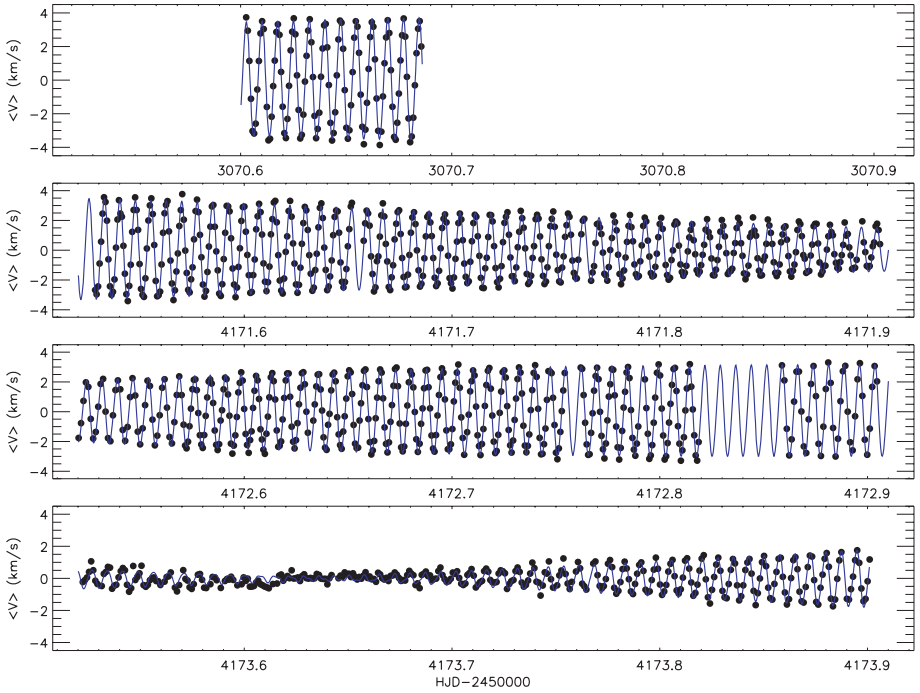

Figure 5. Radial velocities for HD 99563 measured in the line core of Hα for the 2007 observations and the 2004 data (top). Each panel is for a separate night. The data were prewhitened for the rotational mean radial velocity modulations. Superposed in blue is the frequency solution in Table 2 using the distorted oblique dipole nonuplet splitting of ν (1.5576530 mHz).

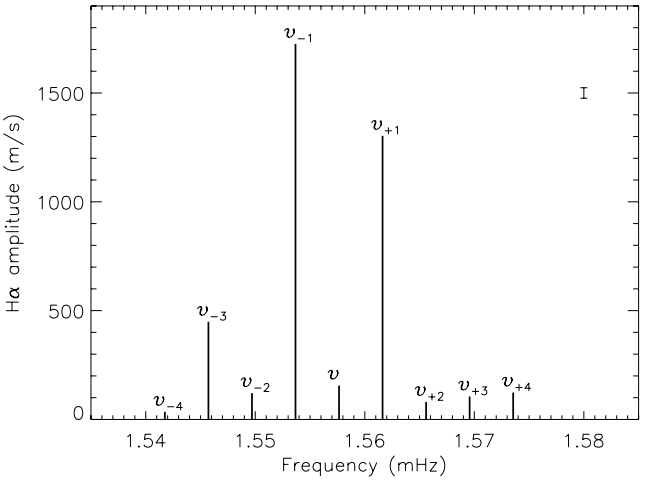

Figure 6. The frequency nonuplet detected in the Hα radial velocity series for HD 99563. Mean amplitude error is indicated with a bar (top, right). Note the multiplet structure is a result of the distorted dipole pulsator geometry, not rotationally perturbed m modes. The frequency splitting is exactly the rotation frequency.

for ν, based on amplitudes and phases in Table 2. The dashed line shows the same, but for a pure dipole triplet pattern only. These are based on the general $(2l + 1)$ multiplet expression in Kurtz (1992) where a linear combination of axisymmetric spherical harmonics is used to describe the observed angular amplitude and phase variations. Amplitudes and phases of the multiplet terms were determined from a fit to the multiplet frequencies from full line profile radial velocity series for that particular line using all spectra. For symmetric lines such as Hα, we used Gaussian fitting. Fig. 7 demonstrates graphically what Table 2 shows numerically. The pulsation mode

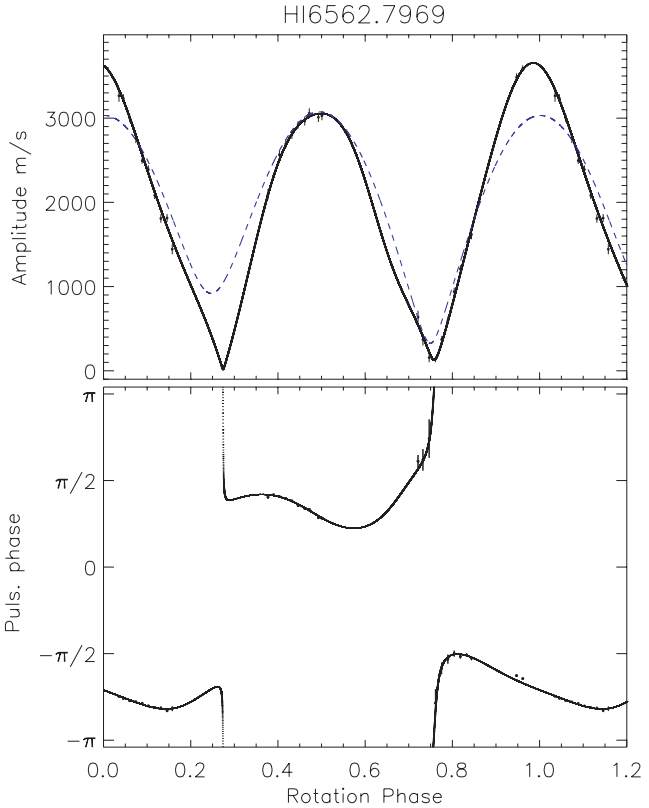

Figure 7. Amplitude and phase variations from Gaussian fits to the line core of Hα. The superposed model in the full line is for a rotationally modulated amplitude nonuplet pattern for ν (see text). For comparison, a pure dipole fit to the frequency triplet only is shown with the dashed (blue) line. The lack of spectra at $\varphi_{\rm rot} = 0.25$ gives the fit too much freedom here.

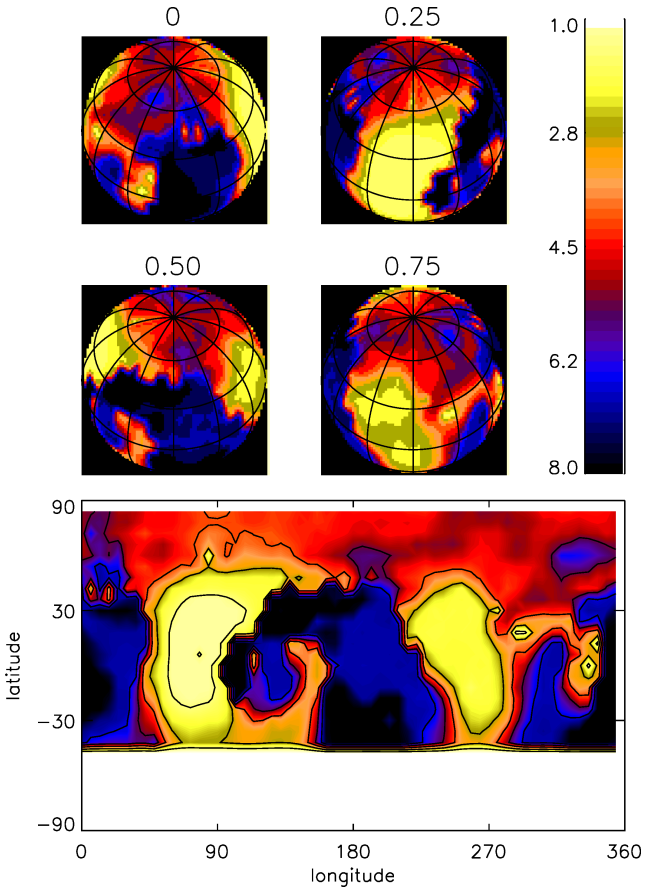

Figure 8. Doppler imaging map for Nd III 6145.07 Å. The abundances are on a scale of $\log N_{\rm H} = 12$; the solar abundance of Nd is 1.41 on this scale (Asplund, Grevesse & Sauval 2005). Thus, the highest overabundances of Nd III in the spots rise to $10^{6.5}$ times solar at the centres of the two spots associated with the magnetic poles. These are evident at rotation phases 0.0 and 0.5, and they lie near the stellar rotational equator (latitude 0°) as a consequence of the magnetic obliquity being near 90° ($\beta = 88°$). The white colour below latitude −44° represents the part of the star that is never visible because of the $i = 44°$ rotational inclination.

is basically an oblique dipole mode, but significant distortion from a simple dipole geometry is required to explain the radial velocity amplitude and phase modulation with rotation for hydrogen.

3.3 Neodymium

This element is very inhomogeneously distributed on the stellar surface. The Doppler imaging map in Fig. 8 shows two concentrated spots, co-located with the magnetic poles as defined at rotation phases 0.0 and 0.5 by Handler et al. In the analysis of Nd, we will first study the frequency content of the Nd lines using the full line profiles, and then study rotational amplitude and phase variations for these two spots. For practical purposes (see e.g. Fig. 10 below), we identify these spots as the *A* (rotational phases 0.2–0.8) and *B* (rotational phases 0.7–1.3) regions.

3.3.1 Observed line profile variations

We find significant partial doubling of the Nd lines during the magnetic crossover phase, which allows us to study the pulsation of two discrete regions of the stellar surface, except for rotation phases

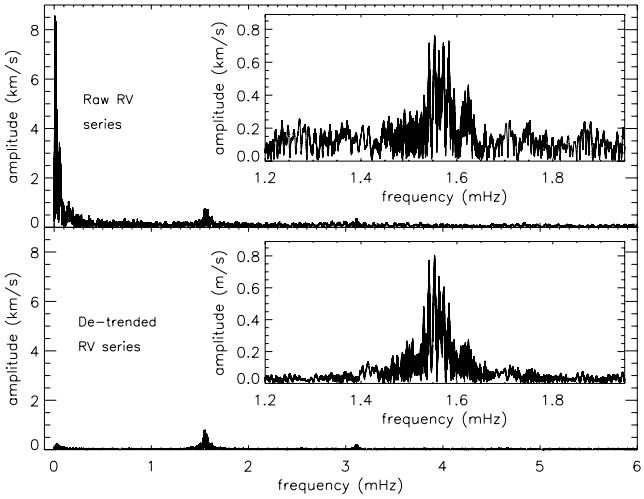

Figure 9. The effect of detrending the 'non-binned' radial velocity curve for Nd III 5102.41 Å. Top panel shows the amplitude spectrum of the raw radial velocity series (with zoom-in panel of the region with the nonuplet pulsational frequency content), while the bottom panel shows the amplitude spectrum for the detrended radial velocity series.

near pulsation maxima when only one or the other spot is visible. Practically, a direct implication of this is that the pulsation amplitude does not go to zero for this element at magnetic quadrature, as it does for Hα. However, as the pulsations in these spots are in antiphase, they would cancel out if we could not resolve their individual line contributions. This concentration of certain ions, such as those of Nd, in spots on HD 99563 (and some other roAp stars) allows us to study the pulsation behaviour of only a part of the visible hemisphere of the star from varying aspect, an opportunity provided by no other kind of pulsating star. Ultimately, this may allow for full 3D mapping of the pulsation velocity field, with the disentangling of horizontal and vertical velocities – important for comparison with theoretical predictions (e.g. Saio 2005).

To evaluate the frequency content in the Nd lines, radial velocities were measured with Gaussian fits to the symmetric Nd lines Nd III 5102.41 Å and Nd III 6327.24 Å, using the full line widths, and they were then combined. Spectra near rotation phase 0.75 were excluded as that is where the *A* and *B* pulsation phases become too mixed, or where one of the components strongly dominates the other.

The radial velocity series for each spot were each detrended with a linear or polynomial fit prior to the frequency analysis (an example of this detrending is shown in Fig. 9). That is justified as the average radial velocities of the two spots shift quasi-linearly with rotation phase, as seen in Fig. 10. A few low frequencies in the range 2–5 c d^{-1} were also included in the least-squares fit to get better error estimates. For the fixed nonuplet frequency solution, as for Hα given in Table 2, we find all components to be significant in Table 3, including $\nu - 4\nu_{\rm rot}$. The residuals show a flat amplitude spectrum with no indication of other pulsation frequencies. Again, as for hydrogen, the many multiplet elements indicate a significantly distorted dipole pulsation.

3.3.2 Pulsation properties from abundance patches

We identified the 'spot' line profile patterns in Fig. 10 as *A* (rotational phases 0.2–0.8) and *B* (rotational phases 0.7–1.3). All spectra were re-measured by fitting Gaussian profiles to the lines, while

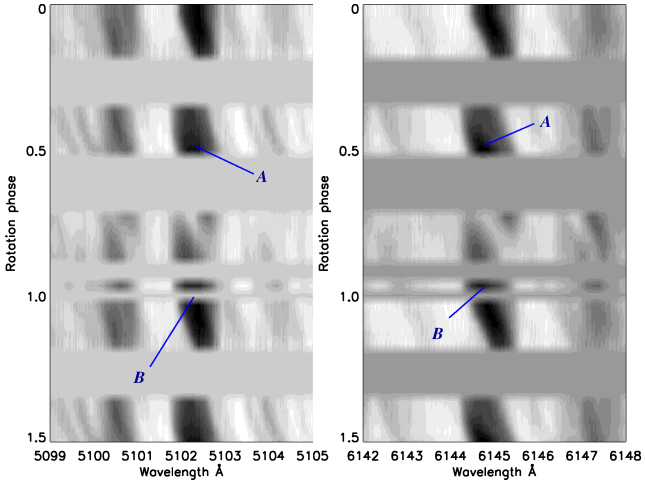

Figure 10. Line region in the vicinities of Nd III 5102.41 Å (left) and Nd III 6145.07 Å (right) shown for all spectra sorted according to rotation phase of HD 99563. The spectra are normalized to unity in the continua (white colour) and absorption features appear dark or black. Four-phase intervals not covered by our high-speed spectroscopic observations appear with a grey-scale corresponding to 0.95. Two-line features relate to the dominant surface patches of high Nd concentration. These are referred to as the *A* (rotational phases 0.2–0.8) and *B* (rotational phases 0.7–1.3) regions.

Table 3. Amplitudes and phases fitted to combined radial velocities of two neodymium lines. The zero-point from Hα in equation (6) was used and the different phases for the two main sidelobes $\nu \pm \nu_{\rm rot}$ correspond to different zero-points for times of maximum amplitude modulation for H and Nd. In fact, this difference in time is 0.19464 d with the Nd maximum coming before the H maximum. This occurs 0.067 earlier in rotation phase, or 24 degrees earlier in rotational longitude – in good agreement with the Nd abundance map, Fig. 8.

Id.	Freq. (mHz)	Amplitude (ms^{-1})	Phase (rad)	S/N
ν	1.5576482	328 ± 64	-0.28 ± 0.20	5.1
$\nu - \nu_{\rm rot}$	1.5536733	1131 ± 71	-2.87 ± 0.06	15.8
$\nu + \nu_{\rm rot}$	1.5616231	531 ± 72	2.57 ± 0.13	7.4
$\nu - 2\nu_{\rm rot}$	1.5496984	445 ± 50	1.09 ± 0.11	8.9
$\nu + 2\nu_{\rm rot}$	1.5655980	456 ± 50	-1.54 ± 0.11	9.1
$\nu - 3\nu_{\rm rot}$	1.5457235	305 ± 43	-1.19 ± 0.14	7.2
$\nu + 3\nu_{\rm rot}$	1.5695729	192 ± 43	-0.68 ± 0.22	4.5
$\nu - 4\nu_{\rm rot}$	1.5417486	230 ± 43	-3.04 ± 0.19	5.3
$\nu + 4\nu_{\rm rot}$	1.5735478	171 ± 43	2.02 ± 0.25	4.0
2ν	3.1152963	77 ± 18	0.68 ± 0.23	4.4
$\nu_{\rm rot}$	0.0039749	134 ± 31	-0.63 ± 0.26	4.4
$2\nu_{\rm rot}$	0.0079498	141 ± 31	1.69 ± 0.23	4.5
$2\nu - 2\nu_{\rm rot}$	3.1073465	158 ± 18	1.13 ± 0.11	8.9

tracing the mean movement of the *A* and *B* features individually with the rotation phase. For time intervals of 1 h, the pulsation amplitude and phase were measured for fixed $\nu = 1.5576482$ mHz, the actual pulsation frequency of the distorted dipole mode.

The two panels in Fig. 11 show the resulting amplitude and phase variations with rotation phase for the two lines Nd III 5102.41 Å and Nd III 6145.07 Å. Measurements for each spot are indicated with different symbols – open boxes for feature *B* and closed circles for feature *A*. Superposed on the figure is a dipole model, constructed using a triplet frequency fit to the full Nd series. Several details are notable in the figure: the pulsation amplitude never reaches zero

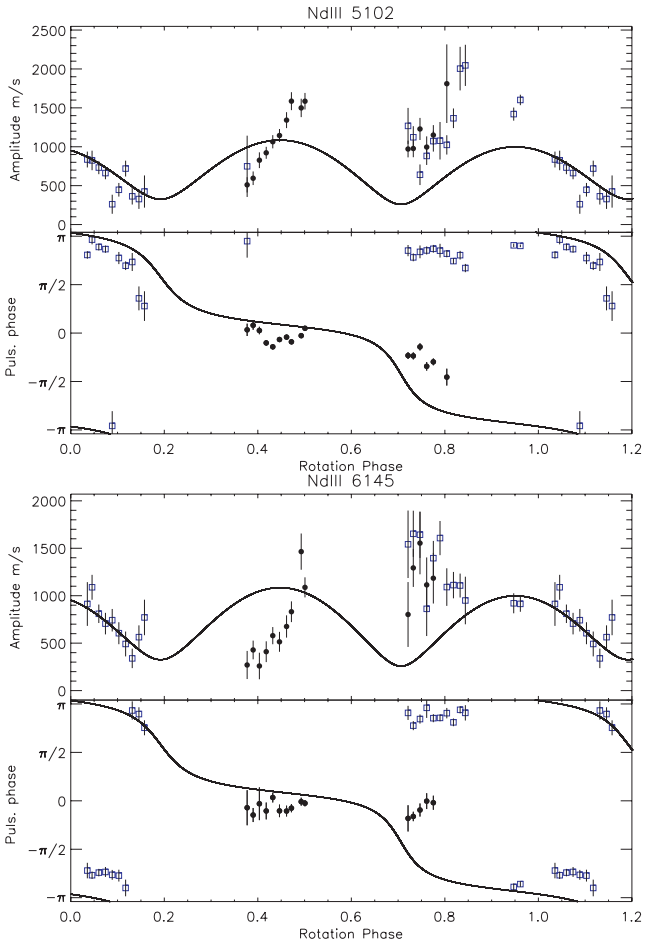

Figure 11. Amplitude and phase variations for Features *A* (closed circles) and *B* (open boxes) in Fig. 10 for Nd III 5102.41 Å (top) and Nd III 6145.07 Å (bottom), measured with Gaussian profile fits. A superposed triplet dipole pattern is shown for comparison with a solid line. The group of measurements near the magnetic crossover phase $\varphi_{\rm rot} = 0.75$ occur during the double-lined phase and show a phase shift near π rad between the two poles, as expected for a basically dipolar pulsation mode.

for any of the spots even when at the stellar limb; the modulated amplitude maximum for spot *A* near rotation phase 0.5 (the spectra only cover the ingress part) is sharper, steeper and shifted in rotation phase with respect to what is expected for a pure dipole model. This is the result of concentration of Nd III towards the magnetic and pulsation poles (see Fig. 8). During quadrature at rotation phase 0.75, it is seen that the pulsation amplitudes for both spots are similar, and about 2/3 of the maximum of the amplitude modulation, a consequence of the projection factor (see below). The increased scatter at this phase is due to line blending between the double-line components, and weaker absorption lines, as the Nd abundance is less overabundant over the visible hemisphere of the star at this phase. Note however, how clearly the pulsation phases divide for the two spots, separated by $\sim\pi$ rad, clearly indicating the global $l = 1$ dipole pulsation.

With both spots at the limb of the star, and with the ability to study them separately, it is interesting to ask whether we can see any evidence of a horizontal component to the pulsations. For example, if the pulsation were purely horizontal, rather than vertical (radial), we would expect to see maximum pulsation amplitude at this rotational phase (0.75) for the Nd III lines. On the other

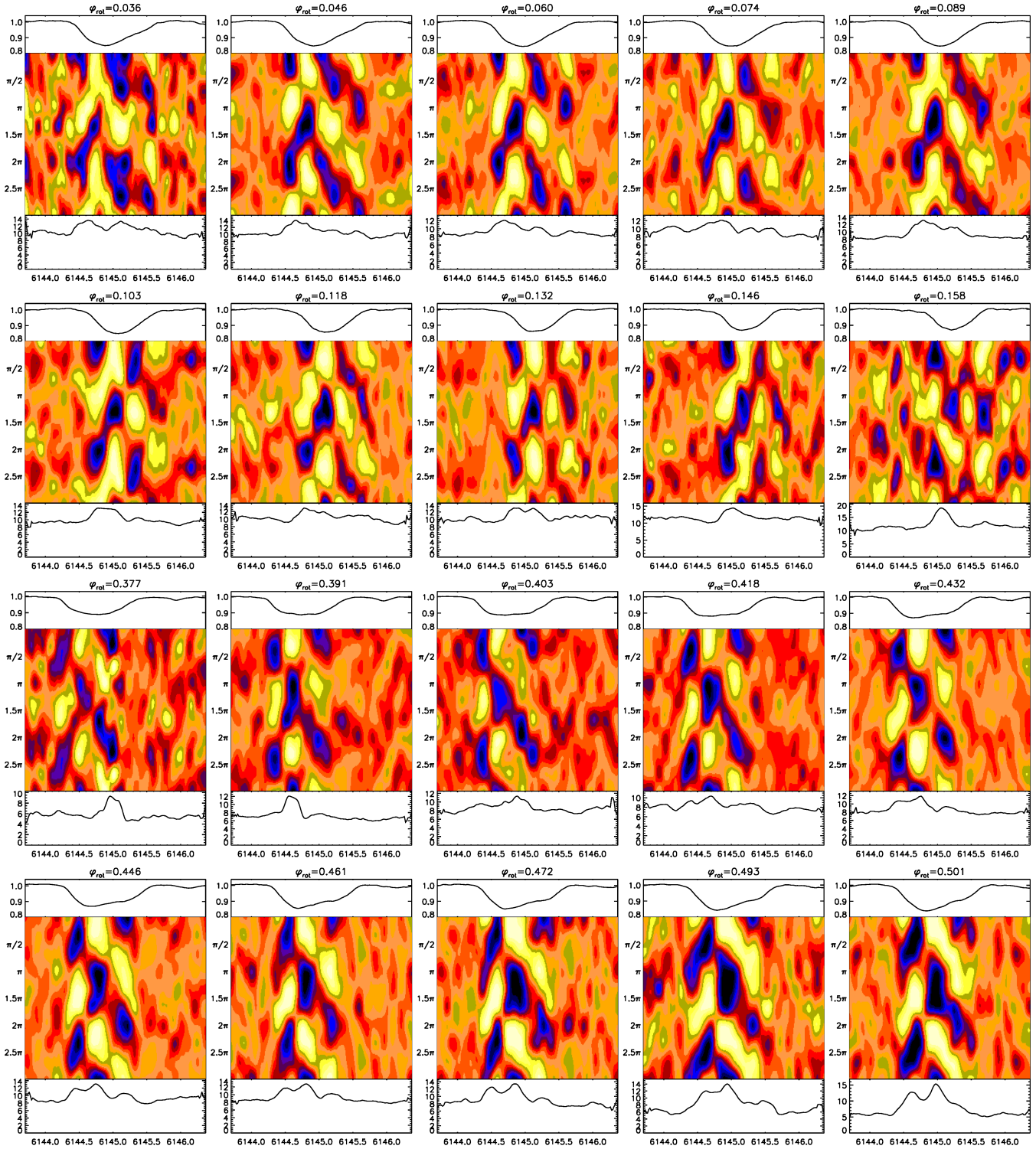

Figure 12. Residual line profile variations in Nd III 6145.07 Å for the 32 time series bins, with rotation phase increasing to the right and downwards, each subtracted from the average spectrum (shown on top of each panel) of that bin. Pulsation phase increases downwards in the middle panels. The standard deviation of each bin series is shown in the bottom of the panels. The colour codes are −0.01 (black) to +0.01 (white) in normalized intensity. Note the clear line doubling for the rotation phases in the top row, observed near the time of magnetic quadrature.

hand, because the Nd III spots are large, there is a component of pulsation in the direction of the line-of-sight for purely vertical pulsation. A simple integral over the half of the visible hemisphere in which a spot is seen (see e.g. Parsons 1972 for the simpler case of Cepheid pulsation) indicates that for purely vertical pulsation velocities we will still expect to see an amplitude about 2/3 that seen at pulsation maximum when the spot is closest to the line-of-sight. This is what we do see in Fig. 11, hence there is no obvious

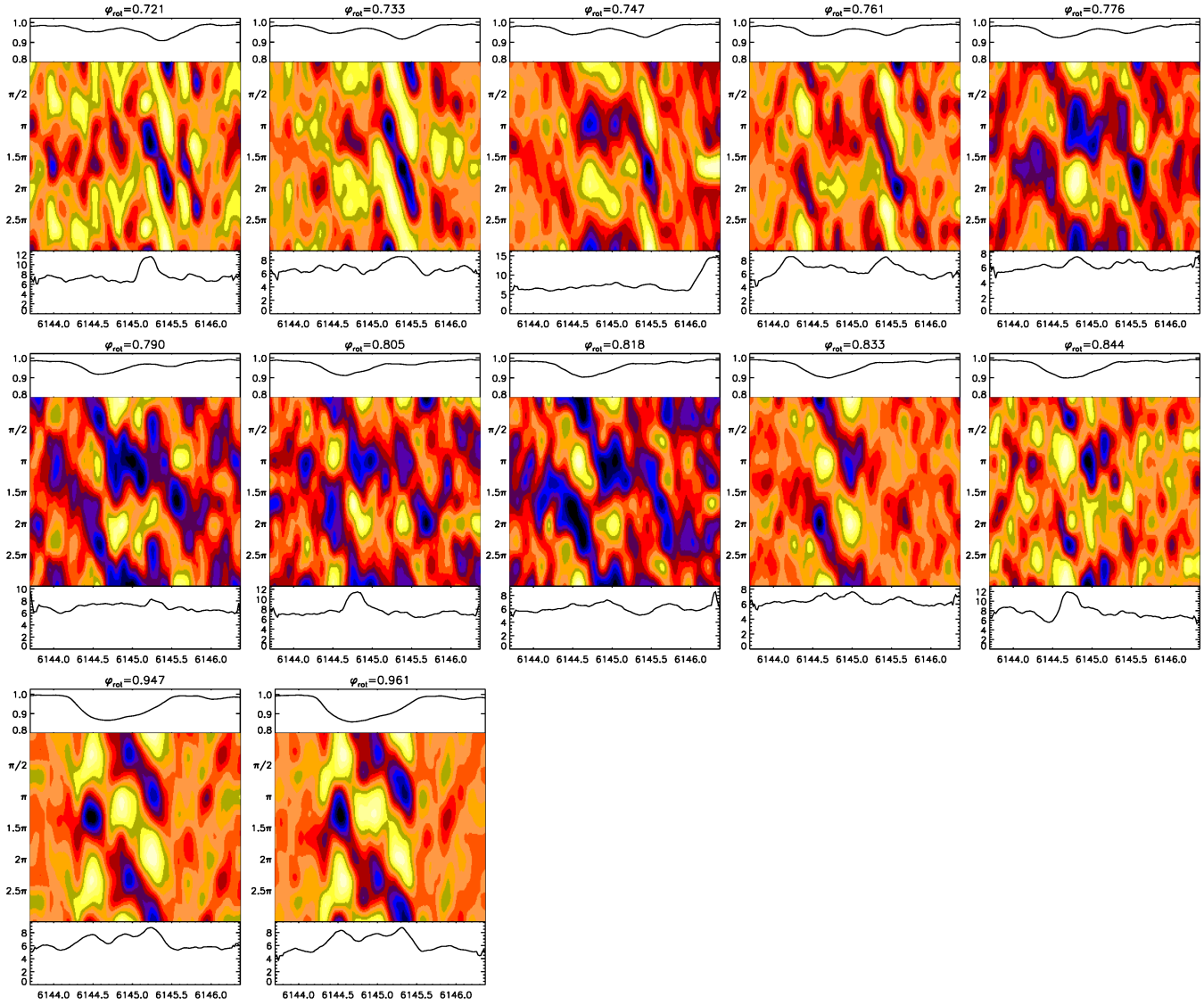

Figure 12 – *continued*

evidence of a horizontal component to the velocity field. We will model this in more detail in a future publication to put limits on the horizontal component. As mentioned in Section 1.3, the horizontal motion goes to zero at the magnetic poles (see e.g. Saio 2005). For large abundance spots, it may still be possible to detect horizontal motion, but the best strategy for detecting such motion may be through the study of abundance spots not centred on the pulsation poles.

Fig. 12 shows the line profile variability in Nd III 6145.07 Å for all 32 1-h bins that we divided the spectra into. Each subpanel shows the average spectrum at this rotation phase, the residual variability for the spectra phased with the pulsation phase progressing downwards. The lower insert of each panel is the standard deviation for the individual series of spectra, pixel-by-pixel. Flux is in all cases in units of normalized flux of the stellar continuum. The figures show a π rad pulsation phase reversal from rotation phase $\varphi_{\rm rot} = 0.0$ to 0.5 (seen as a colour inversion) that can be seen to progress with the stellar rotation.

Recently, Shibahashi et al. (2008) have interpreted blue-to-red running wave features in the line profile variability in the roAp star γ Equ as a manifestation of an upper atmospheric shock wave. Similar blue-to-red features are also seen in the line profile variations of other roAp stars (see e.g. Kochukhov et al. 2007). However, up to now observations have generally been made for short time-spans of typically 2 h and do not cover different rotational phases. An important exception to this is the pioneering study of line profile variability in the roAp star HR 3831 by Kochukhov (2006; see his figs 2 and 3), which shows similarities in the behaviour to that seen in Fig. 12 for HD 99563.

We see in Fig. 12 the line profile variations of a spectral line simply shifting in wavelength without a change of shape at phases near pulsation maximum when the pulsation axis is closest to the line-of-sight, as is expected for a dipole pulsation mode at this aspect. This is clear in the top row of the figure at phase, e.g. $\varphi_{\rm rot} = 0.046$ and other phases near it, and again in the bottom right panel of the figure at phase $\varphi_{\rm rot} = 0.501$. Yet remarkably at magnetic quadrature when the Nd III line is doubled and we can examine the individual components seen at an aspect angle near 90°, there is a clear blue-to-red running wave component visible. Note particularly in Fig. 12 (continued) the upper row of panels and, e.g. $\varphi_{\rm rot} = 0.733$.

This same behaviour was reported first for HR 3831 by Kochukhov (2006) (who also reported red-to-blue features which we possibly see for HD 99563 at some rotation phases, e.g. 0.146 in Fig. 12) and is clearly important for our understanding of these running wave features seen both here and in other roAp stars.

Further interpretation of these features for Nd, as well as for other lines and for other stars, requires modelling of the pulsations, which is work now in progress. Whatever the cause of the blue-to-red running wave line profile variations – whether shock waves as proposed and modelled by Shibahashi et al. (2008), or some other cause – the fact that they are aspect dependent with rotation in HD 99563 and HR 3831 is an important characteristic that needs to be explained.

3.4 Europium

This element shows a highly inhomogeneous surface distribution in the Doppler imaging map seen in Fig. 13. Two circumpolar patches are viewed most favourably near the line-of-sight around $\varphi_{\rm rot} = 0.45$ and 0.95; the third spot is rather concentrated and appears nearest the line-of-sight at $\varphi_{\rm rot} = 0.65$.

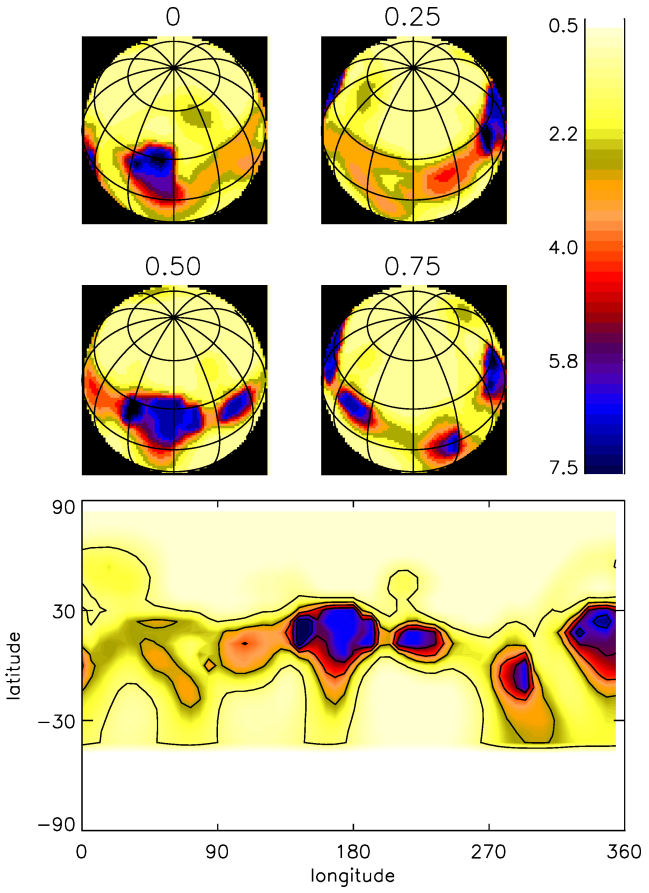

Figure 13. Doppler imaging map for Eu II 6645.06 Å. The abundances are on a scale of $\log N_H = 12$; the solar abundance of Eu is 0.48 on this scale (Asplund et al. 2005). Thus, the highest overabundance of Eu II in the spots rises to 10^7 times solar at the centres of the three spots, two of which are offset from the magnetic and pulsation poles, and the third which is isolated at longitude 290°. The white colour below latitude −44° represents the part of the star that is never visible because of the $i = 44°$ rotational inclination.

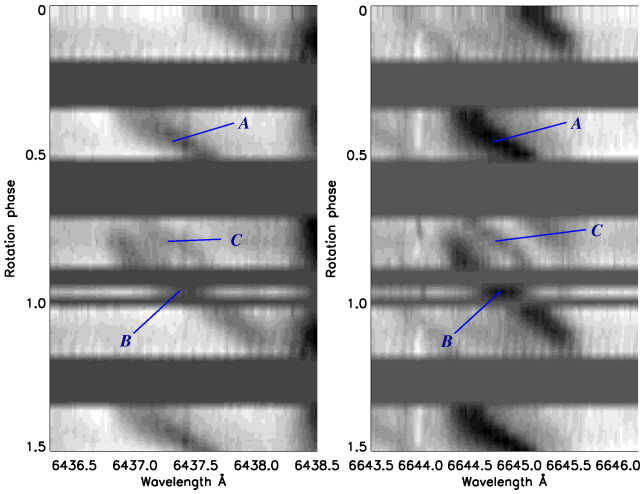

Figure 14. Line region in the vicinities of Eu II 6437.64 Å (left) and Eu II 6645.06 Å (right) shown for all spectra sorted according to rotation phase of HD 99563. Absorption features appear darker and in black. Four-phase intervals were not covered by fast spectroscopy and are shown as smooth dark grey bands. Two-line features relate to dominant surface patches of high Eu concentration. These are referred to as *A* (rotational phases 0.2–0.8) and *B* (0.7–1.3). A third, much more shallow feature is seen at rotational phases 0.7–0.8.

3.4.1 *Observed line profile variations*

In the sequence of spectra in Fig. 14, the two strongest Eu lines Eu II 6437.64 Å and Eu II 6645.06 Å show three moving features which are identified in the figure as *A*, *B* and *C*.

Table 4 shows the results of frequency analyses of three elements, Nd, Eu and Ca. The radial velocities were measured with Gaussian fitting or the CoG procedure (for Ca) to the full line profiles in all spectra. To avoid spectra with mixed contributions, some ∼40 spectra around the magnetic crossover phase ($\varphi = 0.75$) were not used. Detrending for low frequencies was performed with first- and second-order polynomial fitting to spectra dominated by the *A* or *B* features separately (third- and fourth-order polynomials for Eu and Ca) and up to three low frequencies were prewhitened. The results indicate that Nd requires a nonuplet solution and thus has a high distortion to the oblique dipole modulation, while Eu has little power left after a triplet fit. Ca may, however, require at least a quintuplet pattern, but as it has a very low amplitude of a few hundred km s^{-1} (Elkin et al. 2005), the frequencies are not significant when fitting the full nonuplet solution. These results are consistent with the abundance distributions of these elements. The small *A* and *B* spots of Eu do not sample much of the visible hemisphere of the star, except near the poles, so they are fitted well by a simple dipole model. That means that the distortions to the dipolar pulsation that give rise to the other members of the nonuplet for Nd come from regions further from the poles than the Eu samples. These differences may eventually be exploited for more detailed models of the pulsation velocity field. The high 5 km s^{-1} amplitude seen for Eu is consistent with its concentration towards the poles, and may also indicate that it is radiatively stratified to high levels in the atmosphere where the pulsation amplitude is higher. The phase differences (relative to equation 6) of the two main multiplet sidelobes of Eu in Table 4 are, such as shown for Nd, at least partly due to different surface distributions than H.

Table 4. Pulsation amplitudes and phases (φ) fitted to frequencies calculated relatively to a slightly revised ν and to $\nu_{\rm rot}$ in Table 2. The data were detrended for low-frequency trends and low frequencies. The radial velocities were measured using Gaussian fitting, except for lines of calcium where the CoG procedure was used. Note the high amplitude of the Eu lines.

Id.	Amplitude (ms^{-1})	φ (rad)	S/N	Amplitude (ms^{-1})	φ (rad)	S/N	Amplitude (ms^{-1})	φ (rad)	S/N
		Ca I 6439.07 Å			Eu II 6645.06 Å			Eu II 6437.64 Å	
ν	190 ± 139	-1.39 ± 0.72	1.4	452 ± 419	-1.65 ± 0.91	1.1	264 ± 585	1.46 ± 2.21	0.5
$\nu - \nu_{\rm rot}$	409 ± 143	1.46 ± 0.35	2.9	2631 ± 466	-1.59 ± 0.17	5.6	2292 ± 656	-1.18 ± 0.28	3.5
$\nu + \nu_{\rm rot}$	342 ± 144	2.90 ± 0.42	2.4	1996 ± 453	-1.09 ± 0.23	4.4	1931 ± 646	-1.41 ± 0.34	3.0
$\nu - 2\nu_{\rm rot}$	240 ± 100	1.97 ± 0.41	2.4	377 ± 320	0.29 ± 0.85	1.2	488 ± 447	-2.58 ± 0.92	1.1
$\nu + 2\nu_{\rm rot}$	120 ± 99	1.36 ± 0.82	1.2	292 ± 321	0.66 ± 1.10	0.9	941 ± 447	0.10 ± 0.48	2.1
$\nu - 3\nu_{\rm rot}$	263 ± 91	2.62 ± 0.34	2.9	289 ± 275	-0.10 ± 0.94	1.0	271 ± 385	0.69 ± 1.42	0.7
$\nu + 3\nu_{\rm rot}$	95 ± 91	-0.58 ± 0.95	1.1	215 ± 274	2.90 ± 1.27	0.8	784 ± 384	2.38 ± 0.49	2.0
$\nu - 4\nu_{\rm rot}$	203 ± 88	-2.24 ± 0.44	2.3	802 ± 278	2.01 ± 0.34	2.9	120 ± 383	-1.99 ± 3.22	0.3
$\nu + 4\nu_{\rm rot}$	11 ± 88	3.14 ± 8.28	0.1	422 ± 276	1.25 ± 0.66	1.5	689 ± 386	-2.62 ± 0.55	1.8
2ν	95 ± 37	-0.10 ± 0.39	2.6	141 ± 114	-2.85 ± 0.81	1.2	279 ± 160	0.33 ± 0.58	1.7
$2\nu - 2\nu_{\rm rot}$	40 ± 37	-0.10 ± 0.92	1.1	299 ± 114	1.25 ± 0.38	2.6	46 ± 161	2.34 ± 3.50	0.3
		Nd III 5102.41 Å			Nd III 6145.07 Å			Nd III 6327.24 Å	
ν	281 ± 68	-0.29 ± 0.24	4.2	367 ± 186	-0.95 ± 0.51	2.0	267 ± 83	-0.99 ± 0.31	3.2
$\nu - \nu_{\rm rot}$	1000 ± 78	2.78 ± 0.08	12.7	1339 ± 193	-2.89 ± 0.14	6.9	1439 ± 86	-2.73 ± 0.06	16.7
$\nu + \nu_{\rm rot}$	530 ± 78	2.64 ± 0.15	6.8	778 ± 196	1.72 ± 0.25	4.0	282 ± 89	1.52 ± 0.32	3.2
$\nu - 2\nu_{\rm rot}$	318 ± 57	1.16 ± 0.18	5.5	597 ± 132	0.33 ± 0.22	4.5	456 ± 60	0.42 ± 0.13	7.6
$\nu + 2\nu_{\rm rot}$	472 ± 57	-2.43 ± 0.12	8.2	974 ± 134	-1.70 ± 0.14	7.3	480 ± 59	-1.37 ± 0.12	8.1
$\nu - 3\nu_{\rm rot}$	194 ± 47	-1.40 ± 0.24	4.2	339 ± 121	-0.89 ± 0.36	2.8	381 ± 54	-1.44 ± 0.14	7.1
$\nu + 3\nu_{\rm rot}$	242 ± 47	-1.40 ± 0.19	5.2	450 ± 123	-0.67 ± 0.27	3.7	286 ± 54	-0.91 ± 0.19	5.3
$\nu - 4\nu_{\rm rot}$	25 ± 50	0.78 ± 1.97	0.5	305 ± 117	2.49 ± 0.38	2.6	346 ± 52	2.84 ± 0.15	6.6
$\nu + 4\nu_{\rm rot}$	208 ± 50	0.66 ± 0.24	4.2	575 ± 121	1.75 ± 0.21	4.8	340 ± 55	1.96 ± 0.16	6.2
2ν	146 ± 19	1.05 ± 0.13	7.6	113 ± 49	0.33 ± 0.44	2.3	59 ± 22	-0.04 ± 0.37	2.7
$2\nu - 2\nu_{\rm rot}$	147 ± 19	0.83 ± 0.13	7.6	144 ± 49	2.77 ± 0.34	2.9	160 ± 22	1.39 ± 0.14	7.3

3.4.2 Pulsation properties from abundance patches

Angular phase-amplitude variation was studied for the Eu *A* and *B* features in the same manner as done for Nd. The phase differences between Nd and Eu of the *A* and *B* features in Figs. 11 and 15 indicate different surface distributions such that different parts of the pulsation geometry are mapped, consistent with the Doppler imaging maps.

The Eu *C* spot was also studied for angular phase-amplitude variation, but the amplitude was found low and rather constant. This is not surprising, since the *C* spot (see Fig. 13) lies about 40° away from the longitude of the pulsation pole where significantly lower pulsation amplitude is expected for a dipole mode.

4 CONCLUSIONS

We have performed a first analysis of the pulsation of HD 99563 based on one of the most comprehensive spectroscopic efforts on a roAp star so far. We show that the pulsation is well described by a single distorted oblique dipole mode, with different distortion terms for different elements. In the future, we will use these differences to make further inference concerning the pulsation velocity field – ultimately in 3D. By using Doppler imaging maps of the surface distribution of Nd and Eu, we have identified two relatively concentrated spots near the magnetic poles. During rotation phases at magnetic crossover, line doubling in absorption features of these elements (with each component relating to a spot) is considerable, and we show that the stellar photosphere at opposite sides of the star have mutual π rad offset, again supporting the oblique dipole rotator geometry. These spots allow the study of the pulsation mode for only parts of the visible hemisphere of the star, and from varying aspect, an opportunity only possible for roAp stars. Remarkably, blue-to-red running wave features were found only near the rotation phases where the lines were doubled and the spots were seen at high aspect angle.

Our study included a short data set we also obtained with UVES on the VLT 3 yr earlier (Elkin et al. 2005), which after a minor revision of the pulsation frequency showed amplitudes and phases for H, Nd and Eu that in general are consistent with the new data. Some roAp stars exhibit short lifetimes of pulsation modes – in the most extreme case, HD 60435, the mode lifetimes are less than a week. The stability of HD 99563 over a 3-yr time-span simplifies the interpretation of the pulsations. This also suggests that it will be possible to merge future observations of the rotational phases not covered by our data for a more detailed study.

We found a clear rotational variation in the radial velocities of the Hα line in addition to the pulsational variations which we interpret to be the first observational evidence of hydrogen overabundance at the magnetic/pulsational poles, as expected theoretically as a result of helium depletion. While we prefer this interpretation, alternatively, we found the first planet orbiting a roAp star, a hot Jupiter with a mass of 26 times the mass of Jupiter. In future work, we will model the Hα line radial velocity variations in detail to test our preferred hypothesis of hydrogen spots.

ACKNOWLEDGMENTS

LMF, DWK and VGE acknowledge support for this work from the Particle Physics and Astronomy Research Council (PPARC) and from the Science and Technology Facilities Council (STFC). LMF received support from the Danish National Science Research

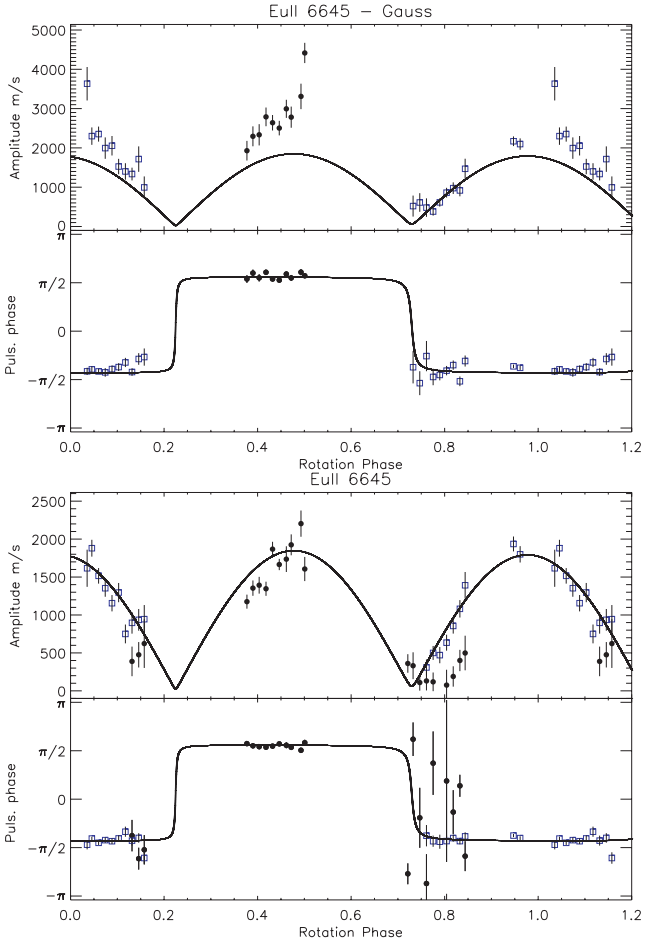

Figure 15. Amplitude and phase variations for features *A* (closed circles) and *B* (open squares) for Eu II 6437.64 Å (top) and Eu II 6645.06 Å (bottom). The line profile fitting was performed using the CoG procedure which gives a lower amplitude than with Gaussian fitting (such as in Fig. 12), but the amplitude exceeds that of Hα. The superposed triplet dipole model was fitted to the radial velocities of the strongest Eu line, Eu II 6645.06 Å. The feature *C* (not shown) was also studied, but had very low amplitude and a high scatter in phases (consistent with its longitude) and has been excluded in this figure for clarity.

Council through the project 'Stellar structure and evolution – new challenges from ground and space observations', carried out at Aarhus University and Copenhagen University. We thank two anonymous referees for helpful comments. We acknowledge extensive usage of the VALD, VizieR, SIMBAD, ADS (NASA) data bases. WZ is supported by the FP6 European Coordination Action HELAS and by the Research Council of the University of Leuven under grant GOA/2003/04.

REFERENCES

Adelman S. J., 1973, ApJ, 183, 95
Ashoka B. N. et al., 2000, Bull. Astron. Soc. India, 28, 251
Asplund M., Grevesse N., Sauval A. J., 2005, in Barnes T. G. III, Bash F. N., eds, ASP Conf. Ser. Vol. 336, Cosmic Abundance as Records of Stellar Evolution and Nucleosynthesis. Astron. Soc. Pac., San Francisco, p. 25
Balmforth N. J., Cunha M. S., Dolez N., Gough D. O., Vauclair S., 2001, MNRAS, 323, 362
Biémont E., Palmeri P., Quinet P., 1999, Ap&SS, 269, 635
Bigot L., Dziembowski W. A., 2002, A&A, 391, 235
Bigot L., Provost J., Berthomieu G., Dziembowski W. A., Goode P. R., 2000, A&A, 356, 218
Bouchy F., Lovis C., Mayor M., Pepe F., Queloz D., Udry S., Melo C., Santos N., 2004, Astron. Soc. Pac. Conf., 321, 15
Breger M. et al., 2005, A&A, 435, 955
Bychkov V. D., Bychkova L. V., Madej J., 2003, A&A, 407, 631
Cunha M. S., 2006, MNRAS, 365, 153 S, 343, 831
Cunha M. S., Gough D., 2000, MNRAS, 319, 1020
Deeming T. J., 1975, Ap&SS, 36, 137
Dorokhova T. N., Dorokhov N. I., 1998, CAOSP, 27, 338
Dorokhova T., Dorokhov N., 2005, JA&A, 26, 223
Dziembowski W. A., Goode P. R., 1996, ApJ, 458, 338
Elkin V. G., Kurtz D. W., Mathys G., 2005, MNRAS, 364, 864
Elkin V. G., Kurtz D. W., Freyhammer L. M., Mathys G., Hubrig S., 2008a, MNRAS, 390, 1250
Elkin V. G., Freyhammer L. M., Kudryavtsev D. O., Romanyuk I. I., 2008b, IBVS, 5851
Fabricius C., Makarov V. V., 2000, A&A, 356, 141
Freyhammer L. M., Kurtz D. W., Mathys G., Elkin V. G., Riley J., 2008a, MNRAS, 385, 1402
Freyhammer L. M., Elkin V. G., Kurtz D. W., 2008b, MNRAS, 390, 257
González J. F., Hubrig S., Kurtz D. W., Elkin V., Savanov I., 2008, MNRAS, 384, 1140
Handler G., Paunzen E., 1999, A&AS, 135, 57
Handler G. et al., 2006, MNRAS, 366, 257
Hubrig S., Kharchenko N., Mathys G., North P., 2000, A&A, 355, 1031
Hubrig S., Szeifert T., Schöller M., Mathys G., Kurtz D. W., 2004, A&A, 415, 685
Hubrig S., North P., Schöller M., Mathys G., 2006, Astron. Nachr., 327, 289
Kochukhov O., 2004, ApJ, 615, L149
Kochukhov O., 2006, A&A, 446, 1051
Kochukhov O., Ryabchikova T., 2001, A&A, 374, 615
Kochukhov O., Ryabchikova T., Weiss W. W., Landstreet J. D., Lyashko D., 2007, MNRAS, 376, 651
Kupka F., Piskunov N., Ryabchikova T. A., Stempels H. C., Weiss W. W., 1999, A&AS, 138, 119 (http://www.astro.uu.se/~vald/)
Kurtz D. W., 1982, MNRAS, 200, 807
Kurtz D. W., 1985, MNRAS, 213, 773
Kurtz D. W., 1992, MNRAS, 259, 701
Kurtz D. W., Martinez P., 2000, Baltic. Astron, 9, 253
Kurtz D. W. et al., 1989, MNRAS, 240, 881
Kurtz D. W., van Wyk F., Roberts G., Marang F., Handler G., Medupe R., Kilkenny D., 1997, MNRAS, 287, 69
Kurtz D. W. et al., 2005, MNRAS, 358, 651
Kurtz D. W., Elkin V. G., Mathys G., 2005c, MNRAS, 358, L6
Kurtz D. W., Elkin V. G., Mathys G., 2006a, MNRAS, 370, 1274
Kurtz D. W., Elkin V. G., Cunha M. S., Mathys G., Hubrig S., Wolff B., Savanov I., 2006b, MNRAS, 372, 286
Kurtz D. W., Elkin V. G., Mathys G., 2006c, in Thompson M., ed., Proc. SOHO 18/GONG 2006/HELAS I, Beyond the Spherical Sun, ESA-SP 624. ESA, Noordwijk, p. 33
Kurtz D. W., Elkin V. G., Mathys G., van Wyk F., 2007, MNRAS, 381, 1301
Lenz P., Breger M., 2005, Commun. Asteroseismol., 146, 53
Martinez P., Kurtz D. W., 1994, MNRAS, 271, 129
Mkrtichian D. E., Hatzes A. P., Kanaan A., 2003, MNRAS, 345, 781
Nelson M. J., Kreidl T. J., 1993, AJ, 105, 1903
Parsons S. B., 1972, ApJ, 174, 57
Piskunov N. E., 1992, in Glagolevsky Yu. V., Romanjuk I. I., eds, Stellar Magnetizm. Nauka, St. Petersburg, p. 92
Preston G. W., 1967, ApJ, 150, 547
Pyper D. M., 1969, ApJS, 18, 347
Ryabchikova T., Piskunov N., Kochukhov O., Tsymbal V., Mittermayer P., Weiss W. W., 2002, A&A, 384, 545
Ryabchikova T., Leone F., Kochukhov O., 2005, A&A, 438, 973
Ryabchikova T. et al., 2007, A&A, 462, 1103
Saio H., 2005, MNRAS, 360, 1022
Saio H., Gautschy A., 2004, MNRAS, 350, 485

Savanov I. S., Malanushenko V. P., Ryabchikova T. A., 1999, Astron. Lett., 25, 802
Savanov I. S., Strassmeier K. G., 2005, A&A, 444, 931
Shibahashi H., Gough D., Kurtz D. W., Kambe E., 2008, PASJ, 60, 63
Sousa S. G., Cunha M. S., 2008, MNRAS, 386, 531
Thompson I. B., Landstreet J. D., 1985, ApJ, 289, L9
Wade G. A., Ryabchikova T. A., Bagnulo S., Piskunov N., 2001, in Mathys G., Solanki S. K., Wickramasinghe D. T., eds, ASP Conf. Ser. Vol. 248, Chemical Satisfaction in Magnetic Ap Stars. Astron. Soc. Pac., San Francisco, p. 373
Weiss W. W., Ryabchikova T. A., Kupka F., Lueftinger T. R., Savanov I. S., Malanushenko V. P., 2000, in Szabados L., Kurtz D., eds, ASP Conf. Ser. Vol. 203, Spectroscopic Survey of Rapidly Oscilating Ap Stars. Astron. Soc. Pac., San Francisco, p. 487
Zima W., 2006, A&A, 455, 227
Zima W., 2008, Commun. Asteroseismol., 155

This paper has been typeset from a TEX/LATEX file prepared by the author.